

Scheduled feeding improves behavioral outcomes and reduces inflammation in a mouse model of Fragile X syndrome.

Huei Bin Wang^{1,3}, Natalie E. Smale³, Sarah H. Brown³, David Zhou³, Aly Mulji², Sophia Anne Marie Villanueva^{2,3}, Kyle Nguyen-Ngo³, John R. Harvey^{2,3}, Cristina A. Ghiani^{3,4}, and Christopher S. Colwell³

¹Molecular, Cellular, Integrative Physiology Graduate Program, ²Integrated Biology and Physiology Program, ³Department of Psychiatry & Biobehavioral Sciences, ⁴Department of Pathology and Laboratory Medicine, David Geffen School of Medicine; University of California Los Angeles.

Funding: Supported by National Institute of Child Health Development under award number: 5U54HD087101 (PI S. Bookheimer).

SHB: 0000-0003-2105-5660

CAG: 0000-0002-9867-6185

CSC: 0000-0002-1059-184X

Corresponding Authors:

Cristina A. Ghiani
Department of Pathology and Laboratory Medicine
University of California Los Angeles
Los Angeles, CA 90024 USA
Email: cghiani@mednet.ucla.edu

Or

Christopher S. Colwell
Department of Psychiatry & Biobehavioral Sciences
University of California Los Angeles
Los Angeles, CA 90024 USA
Email: ccolwell@mednet.ucla.edu

Abstract

Fragile X syndrome (FXS) is a neurodevelopmental disorder caused by the abnormal expansion of CGG repeats in the fragile X mental retardation 1 (FMR1) gene. Many FXS patients experience sleep disruptions, and we sought to explore these symptoms along with the possible benefits of a scheduled feeding intervention using the *Fmr1* knockout (KO) mouse model. These mutants displayed clear evidence for sleep and circadian disturbances including delay in the onset of sleep and fragmented activity rhythms with increases in cycle-to-cycle variability. The *Fmr1* KO mice exhibited deficits in their circadian behavioral response to light with reduced masking, longer time to resetting to shifts in the LD cycle, altered synchronization to a skeleton photoperiod and lower magnitude light-induced phase shifts of activity rhythms. Investigation of the retinal input to the suprachiasmatic nucleus (SCN) with the neurotracer cholera toxin (β subunit) and quantification of the light-evoked cFos expression in the SCN revealed an abnormal retinal innervation of the SCN in the *Fmr1* KO, providing a possible mechanistic explanation for the observed behavioral deficits. Interestingly, disruptions in social and repetitive behavior correlated with sleep duration and fragmentation. Understanding the nature of the deficits, we decided to apply a scheduled feeding regimen (6-hr/18-hr feed/fast cycle) as a circadian-based strategy to boost circadian rhythms independently of light. This intervention significantly improved the activity rhythms and sleep in the mutants. Strikingly, the scheduled feeding ameliorated social interactions and reduced repetitive behaviors as well as the levels of Interferon-gamma and Interleukin-12 in the *Fmr1* KO mutants, suggesting that timed eating may be an effective way to reduce inflammation. Collectively, this work adds support to efforts to develop circadian based interventions to help with symptoms of neurodevelopmental disorders.

Keywords: circadian rhythms, *Fmr1* KO, Fragile X syndrome, inflammation, locomotor activity, neurodevelopmental disorders, scheduled feeding, sleep, time restricted feeding.

Introduction

Fragile X syndrome (FXS) is a neurodevelopmental disorder (NDD) caused by the abnormal expansion of CGG repeats in the fragile X mental retardation 1 (*FMR1*) gene. The trinucleotide repeat expansion causes transcriptional silencing of the *FMR1* gene and reduction in levels of the fragile X mental retardation protein (FMRP), an RNA-binding protein essential for synaptic plasticity among other functions (Zalfa et al., 2006; Soden et al., 2010; Kute et al., 2019). FXS is a relatively common inherited cause of intellectual disability with a prevalence of about 1 in 4,000 males and 1 in 8,000 females (Hersh and Saul, 2011), with the males more severely affected. There is no cure for FXS; current treatments primarily focus on managing the symptoms, among which the most common include social deficits, repetitive behaviors and sleep disruptions (Budimirovic et al., 2022; Mendez and Mendez, 2024). Given the central role of sleep and circadian rhythms in restoration and recovery, a key issue is whether improving the sleep/wake cycle could improve other symptoms of FXS.

Animal models are helpful to better understand the mechanisms underlying circadian and sleep disorders as well as to develop strategies for disease management focused on restoring the sleep/wake cycle. Several models of FXS have been put forward, each with a distinct set of advantages and disadvantages (Sandoval et al., 2024); among them the *Fmr1* knockout (KO) model has been validated for elucidating disease mechanisms and is widely used for preclinical development of drug candidates including those focused on sleep (Thomas et al., 2012; Kazdoba et al., 2014; Kat et al., 2022; Saré et al., 2022; Martinez et al., 2024). Prior work has found that both the *Fmr1/Fxr2* double KO and *Fmr1 KO/Fxr2* heterozygous animals exhibit a loss of rhythmic activity in the light/dark (LD) cycle (Zhang et al., 2008). More recent work has found evidence for deficits in sleep (Saré et al., 2017) and activity (Bonasera et al., 2017; Angelakos et al., 2019) rhythms in the *Fmr1* KO model. This prior work suggest that, like the FSX patients (Kronk et al., 2009; Budimirovic et al., 2022), sleep/wake disturbances can be seen in the mouse models. Still numerous gaps remain in our knowledge in regard to the nature of the deficits and if improving the sleep/disturbances would ameliorate other aspects of the *Fmr1* KO phenotype.

In this study, we sought to comprehensively examine the sleep/circadian disturbances in the *Fmr1* KO mice and to answer the question of whether or not the sleep/circadian disturbances are associated with their behavioral alterations. It is worth noting that much of the literature concerning behavioral deficits in the *Fmr1* KO line were conducted in the middle of the day when the mice were normally asleep, and this daytime protocol may cause sleep disruption. To address this issue, we sought to make use of non-invasive monitoring systems to assess the sleep behavior and the activity rhythms in their home cages, and then we characterized the behavior in their active phase to minimize disruptions to their sleep/wake rhythms. The same mice that were recorded for their sleep/wake cycles were also evaluated with other behavioral tests so that correlations could be examined. Finally, guided by our understanding of the deficits in the *Fmr1* KO line, we utilized a circadian-based intervention (schedule feeding, 6-hr feeding/18-hr fast) and determined its impact on sleep/wake rhythms and well as social deficits, and repetitive behavior.

Methods

Animals

The experimental protocols were approved by the UCLA Animal Research Committee and adhered to the UCLA Division of Laboratory Animal Medicine (DLAM) and National Institute of Health (NIH) guidelines. *Fmr1* KO mice (*Fmr1*^{tm4Cgr}) on the C57BL/6J background (JAX ID: 003025) and wild-type (WT) (JAX ID: 000664) were acquired from the Jackson laboratory (Bar Harbor, ME). The studies were carried out in male adult mice (3 to 5 months old) housed in light-tight ventilated cabinets in temperature- and humidity-controlled conditions, with free access to food and water *ad libitum* except for the experimental groups held on the timed-restricted feeding (TRF) regimen. Mice were individually housed throughout experimental protocols.

Animals tested for social and/or stereotypical behaviors were habituated to the testing room at least 30 mins before the experiments started. The behavioral assays were performed under dim red light (< 2 lx at the level of the testing arena) during the animal active phase, between ZT 16 & 18.

Immobility-Based Sleep Behavior

The sleep behavior under 12h:12h LD cycles was recorded using Anymaze automatic mouse tracking software (Stoelting Co., Wood Dale, IL) that tracked the (40 sec or greater as previously described (Wang et al., 2016; Whittaker et al., 2018)). This threshold was previously determined by Fisher and his colleagues to have 99% correlation with EEG-defined sleep (Fisher et al., 2016). From 5 days of recordings, 2 days with the best recording quality were picked for the analysis. A sleep bout was defined as a time period in which activity stayed above the bout threshold (3 counts of sleep per minute for longer than one minute at a time). Acquiring data were exported in 1-min bins and the total sleep during the light phase and the dark phase was obtained.

Locomotor cage activity rhythms

To characterize the sleep/wake cycles, the WT and the *Fmr1* KO mice were single housed under a scheduled 12h:12h LD cycles. The mice were habituated to this cycle for 2 weeks to ensure entrainment to the appointed LD schedule before activity data was used for analysis. The animals were then released into constant darkness (12h:12h dark-dark, DD) for the assessment of the endogenous rhythms. They were kept in DD for at least 2 weeks with free access to food and water. The locomotor activity under LD cycles and DD was monitored using running wheel sensors that tracked wheel-running activity. In the set of TRF experiments, the locomotor activity rhythms were monitored using a top-mounted passive infra-red (IR) motion detector. Both the wheel-running recordings and the IR recordings were reported to a VitalView data recording system (Mini Mitter, Bend, OR) as previously described. 10 days of recordings were used for analysis and waveform presentations. The analysis was conducted by using the El Temps (A. Diez-Nogura, Barcelona, Spain) and ClockLab (Actimetrics, Lafayette Instruments, Lafayette, IN) programs as previously described (Loh et al., 2014; Lee et al 2018). The periodogram generated by the El Temps provided measures on the period, or the length of one activity cycle, and the power of the rhythmicity. The power, or percent variance (%V), assessed the strength of the mouse's periodicity corrected for activity amount and normalized to variance percent derived from peak significance ($P=0.05$). The fragmentation and the imprecision of daily onset of sleep/wake cycles were determined by the ClockLab. Fragmentation was determined by the number of activity bouts per day (maximum gap: 1 min; threshold 3 counts/min), and the imprecision was determined by calculating the variability of the time of activity onset between the best-fit line of the 10 analyzed days.

Light-regulating circadian behavior

A cohort of age-matched WT and *Fmr1* KO mice were single housed in cages with running wheels under a 12:12 LD cycle (300 lx, 4500K) first and then underwent through four behavioral assays of the photic regulation of the circadian system. (1) Photic suppression on nocturnal activity (negative light masking): mice were exposed to 1 hr of light (300 lx, 4500K) at ZT 14. The number of wheel revolutions during this pulse of white light was compared to the number of wheel revolutions during the equivalent hour collected from the previous day. The fold changes were reported: [(rev during the 1-hr light exposure) – (rev during the dark baseline)]/(rev during the dark baseline) %. (2) Re-entrainment to a 6hr advance of the LD cycle: After stable entrainment, the LD cycles were advanced by 6-hr. The activity was continuously monitored by the wheel-running system and the activity onset determined (VitalView). The re-entrainment was quantified by the

difference between the running activity onset and the new ZT 12 in each recording day. A mouse was determined to be fully entrained when the activity onset was aligned to lights-off and there was no phase shifting for the consecutive 5 days. **(3) Skeleton Photoperiod:** After stable entrainment to the LD 12:12 cycle, mice were placed in a skeleton photoperiod consisting of 1:11: 1:11 LD. The 1-hr light treatments at 300 lx were given at the beginning (ZT 0) and the end (ZT 11) of the original light phase. The mice were kept in this photic condition for at least 2 weeks. Basic activity rhythm parameters were determined (ClockLab). **(4) Light-induced phase shifts to a single exposure to light:** Mice were released into DD for 10 days. The circadian time (CT) of their free-running activity rhythms was determined using VitalView and El Temps software. The time of activity onset under DD was defined as CT 12. On day 11, the mice were exposed to light (300 lx, 4500K, 15 min) at CT 16. After the light pulse, the mice remained in DD for an additional 10 days. The best-fit lines of the activity onsets of sleep/wake cycles before and after the light exposure were measured.

Stereotypic Behavior

The marble burying test was used to evaluate the repetitive digging behavior (Yrigollen et al., 2019). The testing mice were habituated to the testing room for at least 30 mins before the test. An array of 4 marbles by 6 marbles was placed in the testing arena with a layer of 4-cm deep shavings. The testing mouse was introduced to the arena from the corner and allowed to freely behave during the trial. Their behavior was recorded for 30 mins and the testing mouse was carefully returned to their home cages. After the test, the number of buried marbles was counted. Marble buried more than $\frac{2}{3}$ area were counted, and all marbles were cleaned with 70% ethanol before the next use. Time spent on digging was manually scored and the distance travelled was derived from the automatic mouse-tracking system (Anymaze software, Stoelting Co., Wood Dale, IL).

The grooming test was conducted as in our previous work (Wang et al 2020). The behavior of self-grooming was defined as the cleaning, licking, or washing of the limbs, tail, and body surface areas, typically from a head to tail direction, but excluded bouts of scratching. Time spent on self-grooming was manually scored and the distance travelled was derived from the automatic mouse-tracking system (Anymaze software).

Social Behavior

The three-chamber test was performed as previously described (Wang et al 2020; 2022). The testing mice were allowed to freely explore an arena with three chambers where the central chamber remained empty. When being habituated to the three-chamber arena, both the mutants and the WT explored the arena evenly with no preference toward the left or the right chamber (left/right ratio: WT: 0.95 ± 0.14 ; $P = 0.43$ by paired t -test. *Fmr1* KO: 0.82 ± 0.1 ; $P = 0.085$ by paired t -test). The three-chamber test consisted of two parts: the first stage assessed the preference of social approach toward the stranger mouse, and the second stage assessed the ability of social discrimination of the testing mouse. In the first stage (social approach), an up-turned metal-grid pencil cup was placed in the side chambers: one remained empty as the novel object (the object chamber), and a never-met stranger mouse that matched the sex, age, and genotype of the testing mouse was placed in the second up-turned cup (the social chamber). Therefore, the testing mouse was tested for the preference between the object chamber and the social chamber in this first testing stage. In the second stage (social discrimination), the first stranger mouse and the cup remained the same while a second never-met stranger mouse that matched the sex, age, and genotype of the testing mouse was placed in the second up-turned cup. In other words, the social chamber in the first stage became a familiar chamber in the second stage, and the object chamber in the first stage became a novel chamber in the second stage. Thus, the testing mouse was tested for the preference between the familiar chamber and the novel chamber in this second testing stage. Time spent in each chamber and the distance travelled were derived from the automatic mouse-tracking system (Anymaze software).

The 5-trial social test was conducted as previously described (Mineur et al., 2006). The testing mouse was first habituated to a testing arena for 30 mins and then introduced to a never-met stranger mouse for 4 trials. The testing mouse was allowed to explore and interact with the stranger mouse for 2 mins in each trial. A second stranger mouse was introduced to the testing mouse during the 5th trial for 2 mins. The resting interval between trials was 5 mins. Active social behavior such as physical contacts (e.g. crawling over, social grooming), nose-to-nose sniffing, nose-to-anus from the testing mouse to the stranger mice were scored

manually. Testing mice that showed aggressive behavior were withdrawn from the experiment, and the stranger mice showed aggressive behavior were removed from the testing trial and the pool of stranger mice.

Time-restricted feeding (TRF) paradigm

The TRF was conducted as previously described (Wang et al 2018; Whittaker et al 2018; 2023). WT and *Fmr1* KO mice were first entrained to a 12:12 LD (300 lx vs 0 lx respectively) for a minimum of 2 weeks, then were exposed to a feeding paradigm of food (standard chow) available for 6 hr during the middle of the active phase from ZT 15 to ZT 21. Separate cohorts of WT and mutant mice were held on *ad libitum* feeding (ALF). To monitor the sleep/wake cycles, mice were singly housed in cages with an infrared motion sensor. Scheduled feeding was achieved by manually adding and removing food from the mouse cages, and a careful examination was carried out to ensure no small food fragments were dropped and remained in the cages. Food consumption was manually measured by weighing food at the beginning and the end of the feeding cycles (control (ALF): 24 hr vs TRF: 6 hr). The experimental groups and their ALF controls were held in these conditions for a total of 2 weeks.

Injection, Visualisation and Analyses of the Neuroanatomical tracer Cholera Toxin

WT and *Fmr1* KO mice (4 months-old) received a bilateral injection of Cholera Toxin (β subunit) conjugated to Alexa Fluor555 (Life TechnologiesTM, Carlsbad, CA). Prior to the injections, the animals received a drop of a local ophthalmic anesthetic (Proparacaine HCl, 0.5%, Sandoz, Holzkirchen Germany) and an intraperitoneal (i.p.) injection of a non-steroidal anti-inflammatory drug (Carprofen, Zoetis, Parsippany-Troy Hills NJ). The mice were then anesthetized with isoflurane and a 30G needle (BD PrecisionGlideTM Needle; Becton Dickinson, Franklin Lakes NJ) was inserted at a 45° angle into the sclera and the vitreous chamber, towards the base of the retina to allow leakage of vitreous humor. The Cholera Toxin (2 μ g in 2 μ l of sterile PBS) was injected into the vitreous chamber using a 32G Hamilton syringe (Hamilton, Reno NV). The needle was left in place for ten seconds before being retracted. Seventy-two hours after the injection, the mice were euthanized with isoflurane and transcardially perfused with PBS containing 4% PFA. The brains were rapidly dissected out, post-fixed overnight in 4% PFA at 4°C, and cryoprotected in 15% sucrose. Sequential coronal sections (40-50 μ m) containing the left and right suprachiasmatic nuclei (SCN) were mounted, and the coverslips applied with a drop of Vectashield-containing DAPI. Sections were visualized on a Zeiss AxioImager M2 microscope equipped with an AxioCam MRm and the ApoTome imaging system, and images acquired with the Zeiss Zen software and a 10x objective to include both left and right SCN. Two methods of analyses were carried out on the images of 5 consecutive sections per animal containing the middle SCN. First, the relative intensity of the Cholera Toxin fluorescent processes was quantified in the whole SCN, both left and right separately, by scanning densitometry using the Fiji image processing package of the NIH ImageJ software (<https://imagej.net>). A single ROI of fixed size (575.99 μ m x 399.9 μ m, width x height) was used to measure the relative integrated density (mean gray values x area of the ROI) in all the images. The values from the left and right SCN were averaged per section and 5 sections per animal were averaged to obtain one value per animal. Second, the distribution of the Cholera Toxin fluorescent signal was obtained for each left and right SCN separately in the same 4-5 consecutive sections per animal using the Profile Plot Analysis feature of ImageJ. Briefly, a rectangular box of fixed size (415.38 μ m x 110.94 μ m, width x height, **Suppl Fig.1**) to include the ventral part of the SCN was set for each side, and a column plot profile was generated whereby the x-axis represents the horizontal distance through the SCN (lateral to medial for the left and medial to lateral for the right; **Suppl Fig.1**) and the y-axis represents the average pixel intensity per vertical line within the rectangular box. Subsequent processing of the resulting profiles was performed for left and right SCN images separately. To average the profiles of the 5 sections and obtain a single curve per animal, fifth-order polynomial curves were fit to best estimate the position of the intensity peak on the x-axis and, using this position, the original y-axis values were aligned and averaged arithmetically [1 profile per section (either left or right), 5 sections per animal]. Data are shown as the average profile \pm SD of 3 animals per genotype.

Photic induction of cFos in the SCN and cFos-positive Cell Counting

A separate cohort of male WT and *Fmr1* KO mice (3–4 months-old) were housed in DD conditions and exposed to light (300 lx, 4500K, 15 min) at CT 16. Forty-five mins later, the mice were euthanized with isoflurane (30%–32%) and transcardially perfused with phosphate-buffered saline (PBS, 0.1 M, pH 7.4)

containing 4% (w/v) paraformaldehyde (PFA, Sigma). The brains were rapidly dissected out, post-fixed overnight in 4% PFA at 4°C, and cryoprotected in 15% sucrose until further processing. Sequential coronal sections (40-50 µm), containing the middle SCN, were collected on a cryostat (Leica, Buffalo Grove, IL) and further processed for cFos immunofluorescence as previously described (Wang et al., 2017; 2022; Longcore et al., 2024). Briefly, free-floating coronal sections, paired on the rostral-caudal axis and containing both the left and right SCN, were blocked for 1 h at room temperature (1% Bovine Serum Albumin, 0.3% Triton X-100, 10% normal donkey serum in 1xPBS) and then incubated overnight at 4°C with a rabbit polyclonal antiserum against cFos (1:1000, Cell Signaling) followed by a Cy3-conjugated donkey-anti-rabbit secondary antibody (Jackson ImmunoResearch Laboratories, Bar Harbor, ME). Sections were mounted and coverslips applied with Vectashield mounting medium containing DAPI (4'-6-diamidino-2-phenylindole; Vector Laboratories, Burlingame, CA), and visualized on a Zeiss AxioImager M2 microscope (Zeiss, Thornwood NY) equipped with a motorized stage, an AxioCam MRm and the ApoTome imaging system. Z-Stack Images (35 images; 34mm, 1.029mm interval) of both the left and right middle SCN were acquired with a 20X objective using the Zeiss Zen digital imaging software, and two observers masked to the experimental groups performed the cell counting. The boundaries of the SCN were visualized using the DAPI nuclear staining and the cells immunopositive for cFos counted with the aid of the Zen software tool 'marker' in three to five consecutive sections. The numbers obtained from the left and right SCN were averaged to obtain one value per section, and those from three-five sections averaged to obtain one value per animal and are presented as the mean ± standard deviation (SD) of 4 animals per genotype.

Histomorphometrical analyses of the SCN

Photographs of DAPI-stained sections generated from the WT and *Fmr1* KO mice as described above were used to estimate the area, the perimeter, height and width of the SCN as previously reported (Li et al., 2015; Lee et al., 2018). For each animal, the four measurements were performed in three consecutive sections containing the middle SCN and acquired with a 10X objective and the Zen software. Measurements (in µm) of both the left and right SCN were obtained with the auxilium of the AxioVision software (Zeiss, Pleasanton, CA, USA). Because the borders of the DAPI-defined SCN are somewhat arbitrary, measurements were performed independently by two observers masked to the genotype of the animals. The area of the SCN in the three sections was summed, whilst the perimeter, height and width were averaged to obtain one value per side. No significant differences were found between the left and right SCN, therefore the values of the left and right SCN were averaged to obtain one value per animal. Data are shown as the mean ± standard deviation (SD) of 6 animals per genotype.

Blood sampling and measurements of plasma immune molecules

In the beginning of the light phase, blood was collected (~0.5 mL per animal) via cheek puncture into microvette tubes coated with EDTA (Sarstedt, Numbrecht, Germany). Tubes were gently inverted a few times and placed immediately on wet ice. Within 1 h following collection, samples were centrifuged at 2500 rpm for 15 min at 4° C. The plasma was then collected into prelabeled Eppendorf tubes (Fisher Scientific, Hampton, NH), the lids sealed with parafilm, and immediately stored at -80° C until further processing using the Luminex Multiplexed Assay at UCLA (<https://www.uclahealth.org/pathology/services-immunoassays>).

Statistics

Data analyses were performed using SigmaPlot 14.5 or Prism 10 (GraphPad Software, La Jolla, CA). The impact of loss of *Fmrp* on the waveforms of sleep/wake cycles was analyzed using repeated measures two-way analysis of variance (ANOVA) with time and genotype factors. While a two-way ANOVA with genotype and treatment as factors was used for the differences in sleep bouts between light phase and dark phase. The Holm-Sidak's multiple comparisons test was applied after the two-way ANOVA. The datasets were examined for normality (Shapiro–Wilk test) and equal variance (Brown–Forsythe test); genotypic differences in the behavioral tests were determined by Student *t*-test. Correlations between circadian/sleep parameters and other behaviors were examined by applying the Pearson correlation analysis. Normal distribution of the histomorphological datasets and the relative intensity of the Cholera Toxin fluorescent processes in the whole SCN was assessed using the Shapiro-Wilk test. Since the samples did not pass the normality test a two-tailed Mann Whitney test was employed to identify significant differences between groups. The effect of the loss of

FMRP on the photic induction of cFos cells was assessed by one-way ANOVA followed by Bonferroni's multiple comparisons test. Values are reported as the mean \pm standard error of the mean (SEM) or mean \pm standard deviation (SD). Differences were determined significant if $P < 0.05$.

Results

***Fmr1* KOs exhibited shorter and fragmented sleep in the light phase.**

To determine if the *Fmr1* KO had deficits in immobility-defined sleep behavior, the animals were examined using a combination of video recording and mouse tracking system under LD (12:12 hr) conditions. All the mice exhibited robust day-night rhythms in sleep with higher levels of sleep during the day and lowest levels during the first half of the night (**Fig. 1**). Looking at the total sleep values within a 24 hr cycle, the total amount of sleep and the number of sleep bout did not vary with the genotype although the *Fmr1* KO did exhibit a reduction in the average duration of each sleep bout (**Table 1**). A two-way ANOVA used to analyze the temporal pattern of sleep (1-hr bins) of the WT and the mutants indicated significant effects of time ($F_{(23, 287)} = 31.94$; $P < 0.001$) and genotype ($F_{(23, 287)} = 11.95$; $P < 0.001$). A number of diurnal differences emerged when we analyzed day and night sleep parameters with a two-way ANOVA (**Table 1**). Focusing our attention on the day, the *Fmr1* KO mutants exhibited less sleep behavior (**Fig. 1B**) with more bouts of a shorter duration (**Fig. C, D**). In addition, maximum sleep bout duration was about 20 minutes shorter in the mutant mice. The reduced sleep time, shorter bout length, and a greater number of sleep bouts seen during the day are all evidence for a fragmented sleep pattern in the *Fmr1* KO mutants.

***Fmr1* KOs exhibited reduced rhythmic strength and reduced nocturnality.**

Next, we sought to determine if the *Fmr1* KO mice showed deficits in locomotor activity rhythms. The age-matched WT and *Fmr1* KO were housed in running-wheel cages under LD cycles for 2 weeks and then released into DD. All of the mice exhibited a robust daily and circadian rhythms in wheel running activity (**Fig. 2; Table 2**). Under the LD environment, some indication of the commonly reported hyper-activity in the *Fmr1* KO mice emerged (**Fig. 2B**), but activity levels over 24 hrs were not significantly different between the genotypes (**Fig. 2C**). Analysis of the diurnal activity patterns with two-way ANOVA confirmed the significant effects of time ($F_{(23, 287)} = 8.84$; $P = 0.003$) and genotype ($F_{(23, 287)} = 39.75$; $P < 0.001$) on locomotor activity. Under LD conditions (**Fig. 2C**), the mutants exhibited lower power rhythms with increased activity during lights-on and higher cycle-to cycle variability. When the animals were held in DD (**Fig. 2D**), both the WT and the mutants displayed very similar free-running period (τ), but again, the latter presented with weaker rhythmic strength and increased cycle-to-cycle variabilities (**Table 2**). Together, our data suggest that the *Fmr1* KO mice exhibit deficits in the circadian regulation of locomotor activity and specifically raise the possibility of problems in the synchronization to the LD cycle.

***Fmr1* KOs showed difficulties in responding to photic timing cues at behavioral levels.**

We sought to test the possibility that the *Fmr1* KO mice show deficits in their response to light using four behavioral assays with wheel running activity. First, the ability of light (4500K, 50 lx) to suppress or “mask” the locomotor activity of nocturnal mice was evaluated. For this assay, the level of locomotor activity between ZT 14 -15 was first measured under baseline LD conditions. There were no differences between the genotypes (WT: 2229 ± 162 rev; KO: 2639 ± 328 rev; $t_{(18)} = -1.123$, $P = 0.277$). The next day the mice were exposed to light at this same phase and the levels of activity measured. A two-way ANOVA indicated significant effects of genotype ($F_{(1, 39)} = 12.002$; $P = 0.001$) and light exposure ($F_{(1, 39)} = 24.253$; $P < 0.001$). The % suppression of activity by light was higher in the WT compared to the mutants (**Fig. 3A; Table 3**) although a couple of KO mice exhibited levels of masking very similar to WT (**Fig. 3B**). Next, we examined the number of cycles the mice took to re-entrain to a 6 hr phase advance of the LD cycle. While WT mice re-synchronized in 5.9 ± 0.6 days, the *Fmr1* KO took 11.3 ± 0.4 days to adjust to the 6 hr advance (**Fig. 3C, D; Table 3**). Third, we evaluated the entrainment of the mice to a skeleton photoperiod (SPP) in which the full 12-hr of light is replaced by two 1-hr light exposures separated by 11 hr of dark (**Fig. 4A**). In these experiments, the mice were first entrained to the standard LD cycle and then released into the SPP for 2 weeks (**Fig. 4A**). Our recordings demonstrated that the WT controls were able to entrain to this challenging environment and exhibited robust circadian rhythms with a τ of 24.0 ± 0.0 hr (**Table 3**). The *Fmr1* KO exhibited a τ of 23.7 ± 0.2 hr with the shorter period driven by three mutant mice who failed to stably entrain to the SPP (**Table 3**). Compared to the WT controls, the mutants under SPP showed reduced rhythmic strength, increased light-phase activity, and larger cycle-to-cycle onset variability (**Fig. 4B**). Finally, we measured the direct light-induced phase shifts of the circadian system of the mice by exposing them to light (300 lx, CT 16, 15 min) when they were in DD. The WT controls showed a phase delay of 135.6 ± 26.9

min while, in the *Fmr1* KO mutants, the delay in the activity onset the next day was about half the magnitude (64.0 ± 0.1 min) (**Fig. 4C, D; Table 3**). Thus, in all four behavioral tests, we found evidence that the *Fmr1* KO mice exhibited deficits in their circadian light response.

***Fmr1* KOs exhibited subtle deficits in the retinal afferent innervation to the SCN.**

The results described above suggest that *Fmr1* KO mice may exhibit an anomalous retinal input to the SCN. Since the fluorescence-conjugated neurotracer Cholera Toxin (β subunit) has been used to map the projections of melanopsin-expressing intrinsically photoreceptive retinal ganglion cells (ipRGCs) from the retina to the SCN (Muscat et al., 2003; Hattar et al., 2006), the WT and *Fmr1* KO received a bilateral intravitreal injection of this tracer. A lower fluorescent signal could be observed both laterally and medially to the ventral SCN (**Fig. 5A**) as well as beneath in the optic chiasm of the mutant mice as compared to WT. Analysis of the intensity and distribution (**Supp. Fig. 1**) of the labelled retino-hypothalamic processes entering into the ventral SCN showed a reduction particularly evident in the lateral part of both the left and right mutant SCN (**Fig. 5B, C**). Likewise, a subtle decrease in the intensity of the labelled fibers was found in the whole SCN (**Table 4**) of the *Fmr1* KO mice as compared to WT.

A well-established test of the light input to the circadian system is the light-evoked cFos response in the SCN. In line with the results obtained with the Cholera Toxin suggesting an impaired light-pathway to the SCN in the mutants, the number of cFos positive cells in the SCN of the *Fmr1* KO was greatly reduced (50%) in comparison to the WT mice (**Fig. 5D, E; Table 4**). Contrary to other models of neurodevelopmental disabilities (Li et al., 2015; Lee et al., 2018), the *Fmr1* KO mice did not display any histomorphometrical alteration of the SCN (**Table 4**). Based on these findings, we can surmise the presence of an abnormal connectivity between the retina and the SCN in the mutants, which could provide, at least in part, a mechanism for their difficulty in responding to photic cues.

***Fmr1* KOs exhibited deficits in social interactions as well as increased repetitive behaviors**

Social and stereotypic symptoms are hallmark problems in NDDs and we sought to evaluate these behaviors at night (ZT 16-18) in the two genotypes. The active-phase social behavior was first tested with the three-chamber test (**Fig. 6A**). In the first stage of testing, both genotypes showed more interest toward the stranger mouse when they were given the choice between an asocial object and a mouse. The direct comparison of the time spent with the object and the novel mouse did not indicate significant differences between the genotypes (**Table 5**). On the other hand, measurement of the social preference index (SPI) indicated that *Fmr1* KO exhibited reduced interest in conspecifics compared to WT mice (**Table 5**). In the second testing stage, the asocial object was replaced with a second novel mouse and the same stranger mouse from the first stage had become a familiar mouse (**Fig. 6B**). Under these conditions, the *Fmr1* KO spent more time with the familiar mouse than WT (**Table 5**). Again, the social novelty preference index (SNPI) indicated that the *Fmr1* KO exhibited reduced interest in novel mouse compared to WT mice (**Table 5**). The reduced time in exploring and staying in the novel-mouse chamber suggested that the *Fmr1* KO mutants were not able to distinguish the second novel mouse from the first familiar mouse. The possibility of impaired social memory was further tested by the 5-trial social test (**Fig. 6C**). In this test, the first stranger mouse becomes a familiar mouse after 4 exposures to the testing mouse. When the second novel mouse is introduced in the 5th trial, the testing mouse typically shows a boosted interest in investigating the novel mouse. As expected, when the second novel stranger mouse replaced the first familiar mouse and was introduced to the testing animals, WT showed elevated social behavior in the 5th trial. In contrast, the mutants did not show an increased interest in exploring the second novel mouse (**Table 5**).

Next, when the active-phase repetitive behavior was examined by the marble bury test, the *Fmr1* KO spent more time digging and buried more marbles compared to WT (**Fig. 6D, E; Table 5**). When this 30-min trial was divided into three 10-min intervals, the repetitive digging behavior was significant in the *Fmr1* mutants compared with the WT through all three intervals. The two-way ANOVA demonstrated that there was a significant effect of genotype ($F_{(1, 107)} = 11.04$; $P = 0.001$) but not of the interval ($F_{(2, 107)} = 0.42$; $P = 0.66$). The *Fmr1* KO also exhibited significantly more grooming than their WT controls (**Fig. 6F, Table 5**). Finally, we used the data collected to determine if disrupted sleep was correlated with NDD-like behavioral deficits. Significant correlations were found in the social memory tested by the 5-trial social interaction test, the percentage of buried marbles,

and the grooming time (**Table 6**). Sleep duration (**Fig. 6G, H**) and fragmentation (**Fig. 6I, J**) exhibited a moderate-strong correlation with both social recognition and grooming. In addition, we also found moderate correlation between the grooming time and the circadian rhythmic power as well as activity onset variability (**Table 6**). In short, our work demonstrated that even when tested at their circadian active phase, the *Fmr1* KO mice exhibited robust deficits in social memory and repetitive behavior. Moreover, the shorter and the more fragmented the daytime sleep, the more severe the social memory impairment and the repetitive behavior.

A scheduled feeding paradigm ameliorated sleep disturbances and improved the deficits in social memory and repetitive grooming behavior in the Fmr1 KO.

The correlations between the fragmented sleep and the severity of other behavioral phenotypes support the possibility that the interventions focused on improving circadian rhythms and sleep may benefit the observed behavioral deficits in the *Fmr1* KO mice. Scheduled feeding can be a powerful regulator of circadian rhythms (Long and Satchidananda, 2022; Manoogian et al., 2022) and has been shown to be effective in several disease models (Whittaker et al., 2018; Wang et al., 2018; Gao et al., 2022; Gupta et al., 2022; Whittaker et al., 2023). We therefore sought to determine if a scheduled feeding paradigm (TRF: 6-h feeding/18-h fast, 2 weeks of treatment) could benefit the *Fmr1* KO mice. In this study, we compared the 2 genotypes held under *ad libitum* feeding (ALF) as well as TRF. Initially, we confirmed that the food consumption was very similar by the second week (**S. Fig. 2**). Both genotypes were able to learn the protocol and were eating as much as their ALF controls after 5 days. At the end of the two-week treatment, the TRF groups weighed less than the ALF groups (**S. Fig. 2**). The TRF treatment benefited a number of aspects of the temporal patterning of activity and sleep (**Fig. 7**). Notably, the scheduled feeding improved the power of the rhythms along while reducing the fragmentation and cycle-to-cycle variability of the activity rhythms (**Fig. 7C-E; Table 7**). Total cage activity was not altered by the intervention. When the sleep behavior was assessed (**Fig. 7F, G**), the scheduled feeding increased the total amount of daytime sleep in both genotypes (**Fig. 7H; Table 7**), reduced sleep fragmentation (bout #, **Fig. 7I**) and increased the average duration of each bout (**Fig. 7J**). The two-way ANOVA analysis confirmed genotypic differences in the response to TRF with the WT mice showing a more robust sleep response (**Table 7**). During the light phase, the TRF-treated mutants spent more time sleeping with longer sleep bout length and a smaller number of sleep bouts than the ALF controls. The beneficial effects of TRF treatment on sleep behavior were also observed in the WT (**Table 7**). Therefore, TRF benefitted the rhythms in sleep and activity.

We also observed the benefits of TRF treatment on other behaviors in the *Fmr1* KO model. Focusing on social memory and the grooming behavior, we found that TRF improved the memory while reducing the inappropriate grooming behavior (**Table 8**). For these experiments, the social memory was evaluated by the 5-trial social interaction test as described above (**Fig. 8A**). Their social interests in interacting with the second novel mouse were significantly increased to WT-like level, suggesting that the treated mutants were able to distinguish the novel mouse from the familiar mouse. Regarding the repetitive grooming behavior, the TRF-treated *Fmr1* KO mice showed a significant reduction in time spent on self-grooming (**Fig. 8B**). This reduction was not due to any changes in their locomotor ability as there was no feeding effects on the distance travelled during the test among the TRF and ALF groups (**Fig. 8C**). In summary, TRF not only improved the sleep/wake cycles but also the deficits in social memory as well as the self-grooming behavior in the *Fmr1* KO mice.

Scheduled feeding treatment reduced the elevated IL-12 and $INF\gamma$ pathway in the Fmr1 KO mice.

Abnormal immune responses have been suggested to play a role in FXS pathophysiology (Reynolds et al., 2021; Dias et al., 2022; Robinson-Agramonte et al., 2022). To investigate whether the scheduled feeding protocol impacted cytokine profiles in the *Fmr1* KO mice, the plasma samples were collected at the end of the intervention. Our assessment revealed a number of cytokines altered in the mutants, and the changes were countered by TRF (**Table 9**). The comparison within the ALF groups revealed that the mutants had elevated levels of Interleukin-12, (IL-12), Interferon-gamma ($INF\gamma$), and the Chemokine Ligand-9 (CXCL-9) compared to WT. The observed genotypic differences in these pro-inflammatory makers were no longer significant in the TRF-treated groups (**Fig. 9A**). The scheduled feeding also reprinted the levels of IL-2 in the mutant to WT levels. We next asked whether there was a correlation between the levels of these proinflammatory markers and the expression of the behavioral phenotypes. We focused our attention on IL-12 and $INF\gamma$ axis because their levels were elevated in the KO and were successfully reduced by the TRF treatment. Markers of poor sleep such as higher activity in the light phase, shorter sleep time/sleep bout length, and higher numbers of sleep bouts were

significantly associated with higher levels of IL-12 and IFN γ (**Table 10**). The levels of IL-12 and IFN γ were also significantly associated with the social memory impairments and the severity of repetitive grooming behavior (**Fig. 9B,C; Table 10**). Together, our data demonstrate that TRF treatment effectively reduced the levels of pro-inflammatory cytokines in this model of FXS.

Discussion

A significant proportion of individuals with NDDs such as FXS exhibit disruptions to their daily sleep/wake cycles. Particularly common are difficulty falling asleep, staying asleep, and altered sleep patterns (Budimirovic et al., 2022; Minhas et al., 2024), which have a major impact on the quality of life of the patients. Those individuals with the worse set of symptoms in other behaviors also experience the most pronounced sleep problems (Schreck et al., 2004; Taylor et al., 2012; Kaufmann et al., 2024) raising the possibility that the disturbances in the sleep/wake cycle contribute to the severity of other behavioral systems. Notably, abnormalities in sleep are detected early in development even in infants and toddlers carrying the FMR1 mutation (D'Souza et al., 2020). These sleep/wake disruptions may be due to a direct effect of the mutation itself on the circuitry underlying circadian rhythms and sleep homeostasis or indirect effects due to other symptoms including anxiety, sensory hypersensitivity and repetitive behaviors that would themselves disrupt the sleep/wake cycle.

As with other symptoms (Sandoval et al., 2024), animal models are helpful for better understanding the mechanisms underlying circadian and sleep disorders as well as for developing strategies focused on restoring the sleep/wake cycle. In our present study, we used a mouse model to demonstrate that the loss of *Fmr1* had negative impacts on temporal pattern of sleep and locomotor activity with strong deficits in the response to the environment lighting. The disrupted rhythms were significantly associated with the social memory impairments and the repetitive behaviors. Critically, we found that the circadian-based treatment strategy, scheduled feeding, was effective in countering the behavioral deficits as well as reducing the inflammatory signature in the *Fmr1* mutants.

In our behavioral sleep assays, we observed reduced total sleep time and sleep fragmentation in *Fmr1* KO mice (**Fig. 1**). Similarly, Saré and colleagues also found evidence for an impact of the *Fmr1* KO on sleep duration during the light phase using a comparable assay (Saré et al., 2017). Another study (Westmark et al., 2023) examined sleep architecture in the *Fmr1* KO using electroencephalography (EEG). While this work focused on the impact of diet, the control recordings did not find evidence for differences between the *Fmr1* KO and WT controls. We cannot explain the differences between the groups and perhaps this variation suggests that the sleep phenotype is subtle. A gap in this literature is the lack of investigation into sleep homeostatic mechanisms. It is possible that a sleep deprivation protocol could uncover deficits in the *Fmr1* KO model. Notably, these mutant mice display neural oscillation abnormalities, including increased resting state gamma power and heightened amplitude of auditory evoked potentials, paralleling EEG signatures observed in FXS patients (Jonak et al., 2024).

In this study, we assessed diurnal and circadian rhythms in locomotor activity using a wheel-running assay (**Fig. 2**). We observed that *Fmr1* KO mice exhibited weaker rhythms, with increased cycle-to-cycle variation and heightened daytime activity. These disruptions persisted when the mice were housed in DD, where locomotor rhythms are regulated by the circadian system without direct light influence. Previous research has shown that *Fmr1/Fxr2* double KO and *Fmr1 KO/Fxr2* heterozygous mice displayed a marked loss of rhythmic activity under a LD cycle (Zhang et al., 2008). While this early study did report effects in the *Fmr1* KO alone, it did not examine the single mutation in detail. Other studies measuring home cage activity found that *Fmr1* KO mice exhibited significantly reduced movement during their active phase (the dark cycle) and increased bouts of activity during the light cycle compared to WT mice (Bonasera et al., 2017). Similarly, hypoactivity during the night was a prominent feature in male *Fmr1* KO mice, as measured by infrared beam breaks (Angelakos et al., 2019). Collectively, these studies consistently demonstrate disrupted locomotor activity rhythms in *Fmr1* KO mice. The increased daytime activity and greater cycle-to-cycle variability may be attributable to deficits in the light response of the circadian system.

A well-defined circuit mediates the effects of light on circadian system entrainment. The photic signal is detected by intrinsically photosensitive retinal ganglion cells (ipRGCs), which express the photopigment melanopsin (Hattar et al., 2002; Panda et al., 2005). ipRGCs receive input from rod and cone photoreceptors and project to the central circadian clock in the suprachiasmatic nucleus (SCN), as well as to other brain regions involved in cognitive regulation (Lucas et al., 2012; Mahoney and Schmidt, 2024). We conducted a series of experiments to determine if this circuit was compromised in *Fmr1* KO mice (**Figs. 3 & 4**). Behaviorally, we identified deficits in light-evoked suppression of activity (negative masking), the speed of re-entrainment to a new LD cycle, and light-induced phase shifts of the circadian system. A particularly intriguing

assay we used involved exposing the mice to a skeleton photoperiod, consisting of one hour of light followed by 11 hours of darkness. While WT mice readily synchronized to this skeleton photoperiod, *Fmr1* KO mice exhibited several difficulties. These behavioral findings confirmed impairments in light input to the circadian system, prompting further examination of this pathway.

Using fluorescently labeled cholera toxin β (CTB), we demonstrated that ipRGC innervation of the SCN was abnormal in *Fmr1* KO mice (**Fig. 5A**). Additionally, the light-evoked increase in cFos expression in the SCN was reduced in the mutant mice (**Fig. 5B**). Together, the behavioral, anatomical, and functional data suggest deficits in the circadian light response in *Fmr1* KO mice. Since FMRP expression has been reported in ipRGCs (Zhang et al., 2020), these findings may be explained by a loss of function in the retina. Interestingly, these results highlight a reduced circadian light response, contrasting with the general sensory hypersensitivity observed in humans with FXS and *Fmr1* KO models (Rais et al., 2018). It will be important to investigate whether these prominent light input deficits seen in the mouse model are also present in FXS patients. If the circadian light response is indeed compromised, it could have practical implications for the management of FXS.

There was no significant shortening of the free-running circadian period (τ) when activity was measured in DD (**Fig. 2D**; see also Angelakos et al., 2019). The free-running period, as assessed by locomotor behavior in DD, is a highly sensitive marker of the output from the core molecular clock driving circadian oscillations (Takahashi et al., 2008). Furthermore, measurements of clock gene expression in the central clock (SCN) did not reveal any alterations in the rhythmic transcription patterns of core clock genes (*Per1*, *Per2*, *Bmal1*, or *Cry1*) in the *Fmr1* KO mice (Zhang et al., 2008). Given the absence of changes in τ or clock gene expression in the SCN, it is unlikely that the core molecular clock mechanism underlying circadian oscillation is impaired in these mutants. However, our data show that this FXS model exhibits deficits in the photic regulation of the circadian clock and its rhythmic outputs. Although numerous molecular and cellular pathways are impacted by the loss of FMRP, many studies suggest that changes in excitatory/inhibitory (E/I) balance and circuit hyperexcitability may contribute to FXS symptoms. Within the SCN, there is evidence that E/I balance plays a crucial role in network synchronization (Olde Engberink et al., 2023). Therefore, future research should investigate the impact of the *Fmr1* mutation on E/I balance within the SCN. Regardless of the underlying mechanism, the present study demonstrates that *Fmr1* KO mice show disruptions in the temporal patterning of activity and sleep, which aligns with a broader pattern of deficits observed in mouse models of monogenic neurological disorders (Li et al., 2015; Angelakos et al., 2017, 2019; Brown et al., 2019; Shi and Johnson, 2019; Takumi et al., 2019; Wang et al., 2020, 2023).

The *Fmr1* KO mouse model replicates many of the neurological and behavioral deficits observed in FXS (Melancia and Trezza, 2018; Kat et al., 2022). In our study, we demonstrated clear deficits in social recognition and repetitive behaviors, such as excessive grooming. By collecting data on sleep, activity rhythms, and other behaviors from the same animals, we were able to investigate correlations between these behaviors (**Fig. 6**). Based on human data, we hypothesized that individual mice exhibiting the most disrupted sleep would also show the most severe behavioral deficits (Schreck et al., 2004; Taylor et al., 2012; Kaufmann et al., 2024). For instance, one study found that objective sleep and circadian disturbances accounted for approximately 30% of the variance in stereotypic behaviors among ASD patients (Yavuz-Kodat et al., 2020). Consistent with this, we found that mice with the shortest sleep duration, the highest sleep fragmentation, and the weakest rhythm power performed the worst in tests of social recognition and showed the highest levels of repetitive grooming. While these correlations do not establish causation, they align with findings from human studies, which consistently report that individuals with poorer sleep perform worse behaviorally the following day (Robinson-Shelton and Malow, 2016; Budimirovic et al., 2022; Schwichtenberg et al., 2022; Minhas et al., 2024).

A wide range of growing studies have demonstrated that disrupted circadian rhythms and poor sleep lead to a cluster of symptoms, including metabolic deficits, cardiovascular problems, abnormal immune activities, and cognitive deficits (Abdul et al., 2021; Cheng et al., 2021; Johnson et al., 2021; Bisdounis et al., 2022). Many of these same symptoms are seen in FXS and ASD patients (Parente et al., 2022; Protic et al., 2022), indicating a potentially bidirectional link between the circadian clocks and the core NDD symptoms. No

medications are available to treat these core symptoms (i.e., deficits in social communication, sensory aberrations, stereotypic behaviors, and restricted interests). A bidirectional link is exciting as it would raise the possibility of interactions that improve daily rhythms could have therapeutic utility in a variety of NDD conditions. A key test of this hypothesis is to determine if an intervention that improves the sleep/wake cycle in a disease model also improves other phenotypes.

Other research has demonstrated sleep benefits with various dietary interventions. Recent studies have shown that a ketogenic diet (KD) increases NREM sleep and reduces sleep fragmentation while flattening day/night rhythms in *Fmr1* KO mice (Westmark et al., 2024). This same group also found that the KD reduced seizures but did not observe significant KD-responsive effects in several other behavioral tests, such as marble burying, tail suspension, and fear conditioning (Westmark et al., 2020). In our own hands, we found that the KD improved sleep in a mouse model of Huntington's disease (HD) (Whittaker et al., 2022). In this model, improvements in sleep and circadian rhythms paralleled enhanced motor performance. Interestingly, one consequence of placing mice on a KD is the induction of a robust daily rhythm in ketone body levels (Whittaker et al., 2022), suggesting that the KD may function as a type of circadian intervention.

The most common intervention to improve sleep in NDD patients would be to give a sedative before bed. There is a surprising lack of clinical evidence to support this practice or even which hypnotic drug to use. Both clinical and pre-clinical work is needed to address these issues. In the *Fmr1* model, three different classes of hypnotics (zolpidem, ramelteon, DORA-22) were all found to improved sleep (Saré et al., 2022). The rationale behind the use of these different drugs is related to their different pharmacological profiles and mechanisms involved in sleep i.e. zolpidem is a non-benzodiazepine receptor agonist, ramelteon is a melatonin receptor agonist, and DORA-22 is a dual orexin receptor antagonist. Pharmacologically increasing sleep was found to reduce anxiety as measured by the open field but did not improve social behavior. In addition, a recent study used EEG measurements to demonstrate that novel hypnotic (ML297, activator of G-protein-activated inward-rectifying potassium channels) improved increased NREM sleep duration and reduced fragmentation in *Fmr1*-/- mice (Martinez et al., 2024). Importantly, this study was also able to show that this treatment following contextual fear or spatial learning improved memory consolidation in the mutant mice.

We tested the hypothesis that improving sleep and circadian rhythms would alleviate behavioral deficits in *Fmr1* KO mutants using a time-restricted feeding (TRF) protocol. TRF was selected over light therapy due to the deficient responses to photic cues in the *Fmr1* KO mutants. Even after just a two-week treatment, TRF produced significant improvements in the *Fmr1* KO mice. Specifically, TRF enhanced rhythmic power, reduced variability, decreased daytime activity, and lengthened and consolidated sleep bouts during the light phase (**Fig. 7**). Critically, TRF also led to improvements in social memory and reduced repetitive grooming behavior (**Fig. 8**). Previous studies have demonstrated that TRF can improve circadian behavior in aging (Acosta-Rodríguez et al., 2022; Roth et al., 2023) and neurodegenerative models (Wang et al., 2018; Whittaker et al., 2018; 2023). Prior work has shown benefits of intermittent fasting in uncovering and rescuing cognitive phenotypes in the PTEN model of NDD (Cabral-Costa et al., 2018). However, to our knowledge, this is the first demonstration of TRF benefiting a model of NDD.

Our cytokine results (**Fig. 9A**) suggest that inflammation may play a mechanistic role linking improvements in sleep/wake rhythms to reductions in NDD-like behaviors. Altered immune profiles and exaggerated responses to immune challenges have been reported in both FXS patients (Ashwood et al., 2010; Careaga et al., 2014; Van Dijck et al., 2020) and *Fmr1* KO mice (Pacey et al., 2015; Hodges et al., 2020; Bertrand et al., 2021), indicating that the absence of FMRP may contribute to immune system imbalance. In our study, most pro-inflammatory cytokines (>80%) did not vary by genotype (**Table 9**). However, IL-12 (p40) and IFN- γ were elevated in *Fmr1* KO mice and were significantly reduced by the TRF protocol (**Fig. 9A, Table 9**). Notably, we found significant correlations between plasma levels of these two inflammatory markers and the extent of sleep disturbances and behavioral deficits (**Fig. 9B, Table 10**). Similar associations between dysregulated cytokine levels and impaired behavior have been documented in patients and preclinical models (Siniscalco et al., 2018; Matta et al., 2019). For instance, elevated levels of IL-6 and IL-12 are associated with increased stereotypy, cognitive impairments, anxiety, and reduced social interactions in autism spectrum disorder (Konsman et al., 2008; Ashwood et al., 2011; Wei et al., 2012; Fallah et al., 2020). Moreover, counteracting immune dysregulation has been proposed as a strategy to improve behavioral deficits in *Fmr1*

KO mice (Goo et al., 2020). At least one previous study found that TRF reduced inflammatory cytokines in mice (Chen et al., 2023). Whether TRF directly counteracts neuroinflammation in *Fmr1* KO mice remains to be explored, as does the specific role of IL-12 (p40) and IFN- γ in mediating the observed behavioral disruptions. Future studies will be needed to clarify these mechanisms.

Reference

- Abdul F, Sreenivas N, Kommu JVS, Banerjee M, Berk M, Maes M, Leboyer M, Debnath M. Disruption of circadian rhythm and risk of autism spectrum disorder: role of immune-inflammatory, oxidative stress, metabolic and neurotransmitter pathways. *Rev Neurosci*. 2021; 33(1):93-109. doi: 10.1515/revneuro-2021-0022.
- Acosta-Rodríguez V, Rijo-Ferreira F, Izumo M, Xu P, Wight-Carter M, Green CB, Takahashi JS. Circadian alignment of early onset caloric restriction promotes longevity in male C57BL/6J mice. *Science*. 2022; 376(6598):1192-1202. doi: 10.1126/science.abk0297
- Alamilla J, Ramiro-Cortés Y, Mejía-López A, Chavez JL, Rivera DO, Felipe V, Aguilar-Roblero R. Altered Light Sensitivity of Circadian Clock in Shank3+/- Mouse. *Front Neurosci*. 2021;15:604165. doi: 10.3389/fnins.2021.604165.
- Angelakos CC, Tudor JC, Ferri SL, Jongens TA, Abel T. Home-cage hypoactivity in mouse genetic models of autism spectrum disorder. *Neurobiol Learn Mem*. 2019;165:107000. doi: 10.1016/j.nlm.2019.02.010.
- Angelakos CC, Tudor JC, Ferri SL, Jongens TA, Abel T (2019). Home-cage hypoactivity in mouse genetic models of autism spectrum disorder. *Neurobiol Learn Mem* 165, 107000. doi:10.1016/j.nlm.2019.02.010.
- Angelakos CC, Watson AJ, O'Brien WT, Krainock KS, Nickl-Jockschat T, Abel T. Hyperactivity and male-specific sleep deficits in the 16p11.2 deletion mouse model of autism. *Autism Res*. 2017;10(4):572-584. doi: 10.1002/aur.1707.
- Ashwood P, Nguyen DV, Hessel D, Hagerman RJ, Tassone F. Plasma cytokine profiles in Fragile X subjects: is there a role for cytokines in the pathogenesis? *Brain Behav Immun*. 2010 Aug;24(6):898-902. doi: 10.1016/j.bbi.2010.01.008.
- Arsenault, J., Gholizadeh, S., Niibori, Y., Pacey, L. K., Halder, S. K., Koxhioni, E., Konno, A., Hirai, H., & Hampson, D. R. (2016). FMRP Expression Levels in Mouse Central Nervous System Neurons Determine Behavioral Phenotype. *Human gene therapy*, 27(12), 982–996. <https://doi.org/10.1089/hum.2016.090>
- Bisdounis, L., Saunders, K. E. A., Farley, H. J., Lee, C. K., McGowan, N. M., Espie, C. A., & Kyle, S. D. (2022). Psychological and behavioural interventions in bipolar disorder that target sleep and circadian rhythms: A systematic review of randomised controlled trials. *Neuroscience and biobehavioral reviews*, 132, 378–390. <https://doi.org/10.1016/j.neubiorev.2021.12.002>
- Bonasera SJ, Chaudoin TR, Goulding EH, Mittek M, Dunaevsky A. Decreased home cage movement and oromotor impairments in adult Fmr1-KO mice. *Genes Brain Behav*. 2017 16(5):564-573. doi: 10.1111/gbb.12374.
- Brown, L. A., Fisk, A. S., Potheary, C. A., & Peirson, S. N. (2019). Telling the Time with a Broken Clock: Quantifying Circadian Disruption in Animal Models. *Biology (Basel)* 8(1), 18. doi:10.3390/biology8010018
- Budimirovic, D. B., Protic, D. D., Delahunty, C. M., Andrews, H. F., Choo, T. H., Xu, Q., Berry-Kravis, E., Kaufmann, W. E., & FORWARD Consortium (2022). Sleep problems in fragile X syndrome: Cross-sectional analysis of a large clinic-based cohort. *American journal of medical genetics. Part A*, 188(4), 1029–1039. <https://doi.org/10.1002/ajmg.a.62601>
- Cabral-Costa JV, Andreotti DZ, Mello NP, Scavone C, Camandola S, Kawamoto EM. Intermittent fasting uncovers and rescues cognitive phenotypes in PTEN neuronal haploinsufficient mice. *Sci Rep*. 2018;8(1):8595. doi: 10.1038/s41598-018-26814-6.
- Careaga, M., Noyon, T., Basuta, K., Van de Water, J., Tassone, F., Hagerman, R. J., & Ashwood, P. (2014). Group I metabotropic glutamate receptor mediated dynamic immune dysfunction in children with fragile X syndrome. *Journal of neuroinflammation*, 11, 110. <https://doi.org/10.1186/1742-2094-11-110>.
- Chen Y, Li X, Yang M, Wang L, Lv X, Shen K, Wu H, Lu Q. A 2-week time-restricted feeding attenuates psoriasis-like lesions with reduced inflammatory cytokines and immunosenescence in mice. *Exp Dermatol*. 2023 32(11):2000-2011. doi: 10.1111/exd.14932.

- Cheng, W. Y., Lam, K. L., Li, X., Kong, A. P., & Cheung, P. C. (2021). Circadian disruption-induced metabolic syndrome in mice is ameliorated by oat β -glucan mediated by gut microbiota. *Carbohydrate polymers*, 267, 118216. <https://doi.org/10.1016/j.carbpol.2021.118216>
- Colwell CS, Michel S. Sleep and circadian rhythms: do sleep centers talk back to the clock? *Nat Neurosci*. 2003 Oct;6(10):1005-6. doi: 10.1038/nn1003-1005. PMID: 14513032; PMCID: PMC2573023.
- Cohen, S., Fulcher, B. D., Rajaratnam, S. M. W., Conduit, R., Sullivan, J. P., St Hilaire, M. A., Phillips, A. J. K., Loddenkemper, T., Kothare, S. V., McConnell, K., Braga-Kenyon, P., Ahearn, W., Shlesinger, A., Potter, J., Bird, F., Cornish, K. M., & Lockley, S. W. (2018). Sleep patterns predictive of daytime challenging behavior in individuals with low-functioning autism. *Autism research : official journal of the International Society for Autism Research*, 11(2), 391–403. <https://doi.org/10.1002/aur.1899>
- Cristiano, C., Volpicelli, F., Crispino, M., Lacivita, E., Russo, R., Leopoldo, M., Calignano, A., & Perrone-Capano, C. (2022). Behavioral, Anti-Inflammatory, and Neuroprotective Effects of a Novel FPR2 Agonist in Two Mouse Models of Autism. *Pharmaceuticals (Basel, Switzerland)*, 15(2), 161. <https://doi.org/10.3390/ph15020161>
- Dias, C. M., Issac, B., Sun, L., Lukowicz, A., Talukdar, M., Akula, S. K., Miller, M. B., Walsh, K., Rockowitz, S., & Walsh, C. A. (2023). Glial dysregulation in the human brain in fragile X-associated tremor/ataxia syndrome. *Proceedings of the National Academy of Sciences of the United States of America*, 120(23), e2300052120. <https://doi.org/10.1073/pnas.2300052120>.
- D'Souza D, D'Souza H, Horváth K, Plunkett K, Karmiloff-Smith A. Sleep is atypical across neurodevelopmental disorders in infants and toddlers: A cross-syndrome study. *Res Dev Disabil*. 2020 Feb;97:103549. doi: 10.1016/j.ridd.2019.103549.
- El-Ansary, A., & Al-Ayadhi, L. (2014). GABAergic/glutamatergic imbalance relative to excessive neuroinflammation in autism spectrum disorders. *Journal of neuroinflammation*, 11, 189. <https://doi.org/10.1186/s12974-014-0189-0>
- Fallah, H., Sayad, A., Ranjbaran, F., Talebian, F., Ghafouri-Fard, S., & Taheri, M. (2020). IFNG/IFNG-AS1 expression level balance: implications for autism spectrum disorder. *Metabolic brain disease*, 35(2), 327–333. <https://doi.org/10.1007/s11011-019-00510-4>
- Goo, N., Bae, H. J., Park, K., Kim, J., Jeong, Y., Cai, M., Cho, K., Jung, S. Y., Kim, D. H., & Ryu, J. H. (2020). The effect of fecal microbiota transplantation on autistic-like behaviors in Fmr1 KO mice. *Life sciences*, 262, 118497. <https://doi.org/10.1016/j.lfs.2020.118497>
- Gupta, C. C., Vincent, G. E., Coates, A. M., Khalesi, S., Irwin, C., Dorrian, J., & Ferguson, S. A. (2022). A Time to Rest, a Time to Dine: Sleep, Time-Restricted Eating, and Cardiometabolic Health. *Nutrients*, 14(3), 420. <https://doi.org/10.3390/nu14030420>
- Hodges, S. L., Nolan, S. O., Taube, J. H., & Lugo, J. N. (2017). Adult Fmr1 knockout mice present with deficiencies in hippocampal interleukin-6 and tumor necrosis factor- α expression. *Neuroreport*, 28(18), 1246–1249. <https://doi.org/10.1097/WNR.0000000000000905>
- Hodges, S. L., Nolan, S. O., Tomac, L. A., Muhammad, I. D. A., Binder, M. S., Taube, J. H., & Lugo, J. N. (2020). Lipopolysaccharide-induced inflammation leads to acute elevations in pro-inflammatory cytokine expression in a mouse model of Fragile X syndrome. *Physiology & behavior*, 215, 112776. <https://doi.org/10.1016/j.physbeh.2019.112776>.
- Johnson, D. A., Cheng, P., FarrHenderson, M., & Knutson, K. (2023). Understanding the determinants of circadian health disparities and cardiovascular disease. *Chronobiology international*, 40(1), 83–90. <https://doi.org/10.1080/07420528.2021.1966026>.
- Jonak CR, Assad SA, Garcia TA, Sandhu MS, Rumschlag JA, Razak KA, Binder DK. Phenotypic analysis of multielectrode array EEG biomarkers in developing and adult male Fmr1 KO mice. *Neurobiol Dis*. 2024 Jun 1;195:106496. doi: 10.1016/j.nbd.2024.106496..

- Kat R, Arroyo-Araujo M, de Vries RBM, Koopmans MA, de Boer SF, Kas MJH. Translational validity and methodological underreporting in animal research: A systematic review and meta-analysis of the Fragile X syndrome (Fmr1 KO) rodent model. *Neurosci Biobehav Rev*. 2022 Aug;139:104722. doi: 10.1016/j.neubiorev.2022.104722. Epub 2022 Jun 8. PMID: 35690123.
- Kaufmann WE, Raspa M, Bann CM, Gable JM, Harris HK, Budimirovic DB, Lozano R; FORWARD Consortium. Latent Class Analysis Identifies Distinctive Behavioral Subtypes in Children with Fragile X Syndrome. *J Autism Dev Disord*. 2024 Feb;54(2):725-737. doi: 10.1007/s10803-022-05821-7.
- Kazdoba, T. M., Leach, P. T., Silverman, J. L., & Crawley, J. N. (2014). Modeling fragile X syndrome in the Fmr1 knockout mouse. *Intractable & rare diseases research*, 3(4), 118–133. <https://doi.org/10.5582/irdr.2014.01024>
- Kronk, R., Dahl, R., & Noll, R. (2009). Caregiver reports of sleep problems on a convenience sample of children with fragile X syndrome. *American journal on intellectual and developmental disabilities*, 114(6), 383–392. <https://doi.org/10.1352/1944-7588-114.6.383>
- Kronk, R., Bishop, E. E., Raspa, M., Bickel, J. O., Mandel, D. A., & Bailey, D. B., Jr (2010). Prevalence, nature, and correlates of sleep problems among children with fragile X syndrome based on a large scale parent survey. *Sleep*, 33(5), 679–687. <https://doi.org/10.1093/sleep/33.5.679>
- Kute, P. M., Ramakrishna, S., Neelagandan, N., Chattarji, S., & Muddashetty, R. S. (2019). NMDAR mediated translation at the synapse is regulated by MOV10 and FMRP. *Molecular brain*, 12(1), 65. <https://doi.org/10.1186/s13041-019-0473-0>
- Lee FY, Wang HB, Hitchcock ON, Loh DH, Whittaker DS, Kim YS, Aiken A, Kokikian C, Dell'Angelica EC, Colwell CS, Ghiani CA. Sleep/Wake Disruption in a Mouse Model of BLOC-1 Deficiency. *Front Neurosci*. 2018 Nov 15;12:759. doi: 10.3389/fnins.2018.00759.
- Li Q, Loh DH, Kudo T, Truong D, Derakhshesh M, Kaswan ZM, Ghiani CA, Tsoa R, Cheng Y, Sun YE, Colwell CS. Circadian rhythm disruption in a mouse model of Rett syndrome circadian disruption in RTT. *Neurobiol Dis*. 2015;77:155-64. doi: 10.1016/j.nbd.2015.03.009.
- Liu, X., Kumar, V., Tsai, N. P., & Auerbach, B. D. (2022). Hyperexcitability and Homeostasis in Fragile X Syndrome. *Frontiers in molecular neuroscience*, 14, 805929. <https://doi.org/10.3389/fnmol.2021.805929>.
- Loh DH, Kuljis DA, Azuma L, Wu Y, Truong D, Wang HB, Colwell CS. Disrupted reproduction, estrous cycle, and circadian rhythms in female mice deficient in vasoactive intestinal peptide. *J Biol Rhythms*. 2014 Oct;29(5):355-69. doi: 10.1177/0748730414549767.
- Long, H., & Panda, S. (2022). Time-restricted feeding and circadian autophagy for long life. *Nature reviews. Endocrinology*, 18(1), 5–6. <https://doi.org/10.1038/s41574-021-00600-3>
- Lucas RJ, Lall GS, Allen AE, Brown TM. How rod, cone, and melanopsin photoreceptors come together to enlighten the mammalian circadian clock. *Prog Brain Res*. 2012;199:1-18. doi: 10.1016/B978-0-444-59427-3.00001-0.
- Mahoney HL, Schmidt TM. The cognitive impact of light: illuminating ipRGC circuit mechanisms. *Nat Rev Neurosci*. 2024 Mar;25(3):159-175. doi: 10.1038/s41583-023-00788-5.
- Martinez JD, Wilson LG, Brancaleone WP, Peterson KG, Popke DS, Garzon VC, Perez Tremble RE, Donnelly MJ, Mendez Ortega SL, Torres D, Shaver JJ, Jiang S, Yang Z, Aton SJ. Hypnotic treatment improves sleep architecture and EEG disruptions and rescues memory deficits in a mouse model of fragile X syndrome. *Cell Rep*. 2024 Jun 25;43(6):114266. doi: 10.1016/j.celrep.2024.114266.
- Malow, B. A., Adkins, K. W., Reynolds, A., Weiss, S. K., Loh, A., Fawkes, D., Katz, T., Goldman, S. E., Madduri, N., Hundley, R., & Clemons, T. (2014). Parent-based sleep education for children with autism spectrum disorders. *Journal of autism and developmental disorders*, 44(1), 216–228. <https://doi.org/10.1007/s10803-013-1866-z>

Manoogian, E. N. C., Chow, L. S., Taub, P. R., Laferrère, B., & Panda, S. (2022). Time-restricted Eating for the Prevention and Management of Metabolic Diseases. *Endocrine reviews*, 43(2), 405–436. <https://doi.org/10.1210/edrev/bnab027>

Matta, S. M., Hill-Yardin, E. L., & Crack, P. J. (2019). The influence of neuroinflammation in Autism Spectrum Disorder. *Brain, behavior, and immunity*, 79, 75–90. <https://doi.org/10.1016/j.bbi.2019.04.037>

Melancia F, Trezza V. Modelling fragile X syndrome in the laboratory setting: A behavioral perspective. *Behav Brain Res*. 2018 Sep 17;350:149-163. doi: 10.1016/j.bbr.2018.04.042.

Mineur, Y. S., Huynh, L. X., & Crusio, W. E. (2006). Social behavior deficits in the Fmr1 mutant mouse. *Behavioural brain research*, 168(1), 172–175. <https://doi.org/10.1016/j.bbr.2005.11.004>.

Minhas A, Whitlock K, Rosenfelt C, Shatto J, Finlay B, Zwicker J, Lippe S, Jacquemont S, Hagerman R, Murias K, Bolduc FV. Analyzing the Quality of Life in Individuals with Fragile X Syndrome in Relation to Sleep and Mental Health. *J Autism Dev Disord*. 2024 Apr 23. doi: 10.1007/s10803-024-06317-2.

Olde Engberink, A. H. O., de Torres Gutiérrez, P., Chiosso, A., Das, A., Meijer, J. H., & Michel, S. (2023). Aging affects GABAergic function and calcium homeostasis in the mammalian central clock. *Frontiers in neuroscience*, 17, 1178457. <https://doi.org/10.3389/fnins.2023.1178457>.

Pacey, L. K., Guan, S., Tharmalingam, S., Thomsen, C., & Hampson, D. R. (2015). Persistent astrocyte activation in the fragile X mouse cerebellum. *Brain and behavior*, 5(10), e00400. <https://doi.org/10.1002/brb3.400>.

Pandi-Perumal, S. R., Cardinali, D. P., Zaki, N. F. W., Karthikeyan, R., Spence, D. W., Reiter, R. J., & Brown, G. M. (2022). Timing is everything: Circadian rhythms and their role in the control of sleep. *Frontiers in neuroendocrinology*, 66, 100978. <https://doi.org/10.1016/j.yfrne.2022.100978>.

Park, G., Jeon, S. J., Ko, I. O., Park, J. H., Lee, K. C., Kim, M. S., Shin, C. Y., Kim, H., & Lee, Y. S. (2022). Decreased in vivo glutamate/GABA ratio correlates with the social behavior deficit in a mouse model of autism spectrum disorder. *Molecular brain*, 15(1), 19. <https://doi.org/10.1186/s13041-022-00904-z>.

Parente, M., Tonini, C., Buzzelli, V., Carbone, E., Trezza, V., & Pallottini, V. (2022). Brain Cholesterol Biosynthetic Pathway Is Altered in a Preclinical Model of Fragile X Syndrome. *International journal of molecular sciences*, 23(6), 3408. <https://doi.org/10.3390/ijms23063408>.

Petroni, V., Subashi, E., Premoli, M., Wöhr, M., Crusio, W. E., Lemaire, V., & Pietropaolo, S. (2022). Autistic-like behavioral effects of prenatal stress in juvenile Fmr1 mice: the relevance of sex differences and gene-environment interactions. *Scientific reports*, 12(1), 7269. <https://doi.org/10.1038/s41598-022-11083-1>.

Protic, D. D., Aishworiya, R., Salcedo-Arellano, M. J., Tang, S. J., Milisavljevic, J., Mitrovic, F., Hagerman, R. J., & Budimirovic, D. B. (2022). Fragile X Syndrome: From Molecular Aspect to Clinical Treatment. *International journal of molecular sciences*, 23(4), 1935. <https://doi.org/10.3390/ijms23041935>.

Rais M, Binder DK, Razak KA, Ethell IM. Sensory Processing Phenotypes in Fragile X Syndrome. *ASN Neuro*. 2018;10:1759091418801092. doi: 10.1177/1759091418801092.

Reynolds, K. E., Krasovska, V., & Scott, A. L. (2021). Converging purinergic and immune signaling pathways drive IL-6 secretion by Fragile X cortical astrocytes via STAT3. *Journal of neuroimmunology*, 361, 577745. <https://doi.org/10.1016/j.jneuroim.2021.577745>.

Robinson-Agramonte, M. L. A., Noris García, E., Fraga Guerra, J., Vega Hurtado, Y., Antonucci, N., Semprún-Hernández, N., Schultz, S., & Siniscalco, D. (2022). Immune Dysregulation in Autism Spectrum Disorder: What Do We Know about It?. *International journal of molecular sciences*, 23(6), 3033. <https://doi.org/10.3390/ijms23063033>.

Robinson-Shelton, A., & Malow, B. A. (2016). Sleep Disturbances in Neurodevelopmental Disorders. *Current psychiatry reports*, 18(1), 6. <https://doi.org/10.1007/s11920-015-0638-1>

- Roth JR, Varshney S, de Moraes RCM, Melkani GC. Circadian-mediated regulation of cardiometabolic disorders and aging with time-restricted feeding. *Obesity (Silver Spring)*. 2023 Feb;31 Suppl 1(Suppl 1):40-49. doi: 10.1002/oby.23664.
- Sandoval, S. O., Méndez-Albelo, N. M., Xu, Z., & Zhao, X. (2024). From wings to whiskers to stem cells: why every model matters in fragile X syndrome research. *Journal of neurodevelopmental disorders*, 16(1), 30. <https://doi.org/10.1186/s11689-024-09545-w>.
- Saré RM, Lemons A, Smith CB. Effects of Treatment With Hypnotics on Reduced Sleep Duration and Behavior Abnormalities in a Mouse Model of Fragile X Syndrome. *Front Neurosci*. 2022 Jun 2;16:811528. doi: 10.3389/fnins.2022.811528.
- Saré RM, Harkless L, Levine M, Torossian A, Sheeler CA, Smith CB. Deficient Sleep in Mouse Models of Fragile X Syndrome. *Front Mol Neurosci*. 2017 10:280. doi: 10.3389/fnmol.2017.00280
- Schreck, K. A., Mulick, J. A., & Smith, A. F. (2004). Sleep problems as possible predictors of intensified symptoms of autism. *Research in developmental disabilities*, 25(1), 57–66. <https://doi.org/10.1016/j.ridd.2003.04.007>.
- Schwichtenberg AJ, Janis A, Lindsay A, Desai H, Sahu A, Kellerman A, Chong PLH, Abel EA, Yacilla JK. Sleep in Children with Autism Spectrum Disorder: A Narrative Review and Systematic Update. *Curr Sleep Med Rep*. 2022;8(4):51-61. doi: 10.1007/s40675-022-00234-5.
- Siniscalco, D., Schultz, S., Brigida, A. L., & Antonucci, N. (2018). Inflammation and Neuro-Immune Dysregulations in Autism Spectrum Disorders. *Pharmaceuticals (Basel, Switzerland)*, 11(2), 56. <https://doi.org/10.3390/ph11020056>.
- Sørensen, E. M., Bertelsen, F., Weikop, P., Skovborg, M. M., Banke, T., Drasbek, K. R., & Scheel-Krüger, J. (2015). Hyperactivity and lack of social discrimination in the adolescent Fmr1 knockout mouse. *Behavioural pharmacology*, 26(8 Spec No), 733–740. <https://doi.org/10.1097/FBP.000000000000152>.
- Shi SQ, Johnson CH (2019). Circadian biology and sleep in monogenic neurological disorders and its potential application in drug discovery. *Curr Opin Behav Sci* 25, 23-30. doi:10.1016/j.cobeha.2018.06.006.
- Sikora, D. M., Johnson, K., Clemons, T., & Katz, T. (2012). The relationship between sleep problems and daytime behavior in children of different ages with autism spectrum disorders. *Pediatrics*, 130 Suppl 2, S83–S90. <https://doi.org/10.1542/peds.2012-0900F>.
- Soden, Marta E., and Lu Chen. "Fragile X protein FMRP is required for homeostatic plasticity and regulation of synaptic strength by retinoic acid." *Journal of Neuroscience* 30.50 (2010): 16910-16921.
- Takumi T, Tamada K, Hatanaka F, Nakai N, Bolton PF (2019). Behavioral neuroscience of autism. *Neurosci Biobehav Rev*. pii, S0149-7634(18)30372-5. doi:10.1016/j.neubiorev.2019.04.012.
- Taylor, M. A., Schreck, K. A., & Mulick, J. A. (2012). Sleep disruption as a correlate to cognitive and adaptive behavior problems in autism spectrum disorders. *Research in developmental disabilities*, 33(5), 1408–1417. <https://doi.org/10.1016/j.ridd.2012.03.013>.
- Thomas AM, Bui N, Perkins JR, Yuva-Paylor LA, Paylor R. Group I metabotropic glutamate receptor antagonists alter select behaviors in a mouse model for fragile X syndrome. *Psychopharmacology (Berl)* 2012; 219:47 – 58.
- Van Dijck, A., Barbosa, S., Bermudez-Martin, P., Khalfallah, O., Gilet, C., Martinuzzi, E., Elinck, E., Kooy, R. F., Glaichenhaus, N., & Davidovic, L. (2020). Reduced serum levels of pro-inflammatory chemokines in fragile X syndrome. *BMC neurology*, 20(1), 138. <https://doi.org/10.1186/s12883-020-01715-2>.
- Wang HB, Loh DH, Whittaker DS, Cutler T, Howland D, Colwell CS. Time-Restricted Feeding Improves Circadian Dysfunction as well as Motor Symptoms in the Q175 Mouse Model of Huntington's Disease. *eNeuro*. 2018; 5(1):ENEURO.0431-17.2017. doi: 10.1523/ENEURO.0431-17.2017.

- Wang HB, Whittaker DS, Truong D, Mulji AK, Ghiani CA, Loh DH, Colwell CS. Blue light therapy improves circadian dysfunction as well as motor symptoms in two mouse models of Huntington's disease. *Neurobiol Sleep Circadian Rhythms*. 2017 Jan 20;2:39-52. doi: 10.1016/j.nbscr.2016.12.002.
- Westmark, P. R., Gutierrez, A., Gholston, A. K., Wilmer, T. M., & Westmark, C. J. (2020). Preclinical testing of the ketogenic diet in fragile X mice. *Neurochemistry international*, 134, 104687. <https://doi.org/10.1016/j.neuint.2020.104687>.
- Westmark PR, Gholston AK, Swietlik TJ, Maganti RK, Westmark CJ. Ketogenic Diet Affects Sleep Architecture in C57BL/6J Wild Type and Fragile X Mice. *Int J Mol Sci*. 2023; 24(19):14460. doi: 10.3390/ijms241914460.
- Westmark PR, Swietlik TJ, Runde E, Corsiga B, Nissan R, Boeck B, Granger R, Jennings E, Nebbia M, Thauwald A, Lyon G, Maganti RK, Westmark CJ. Adult Inception of Ketogenic Diet Therapy Increases Sleep during the Dark Cycle in C57BL/6J Wild Type and Fragile X Mice. *Int J Mol Sci*. 2024; 25(12):6679. doi: 10.3390/ijms25126679.
- Whittaker, D. S., Akhmetova, L., Carlin, D., Romero, H., Welsh, D. K., Colwell, C. S., & Desplats, P. (2023). Circadian modulation by time-restricted feeding rescues brain pathology and improves memory in mouse models of Alzheimer's disease. *Cell metabolism*, 35(10), 1704–1721.e6. <https://doi.org/10.1016/j.cmet.2023.07.014>.
- Whittaker DS, Loh DH, Wang HB, Tahara Y, Kuljis D, Cutler T, Ghiani CA, Shibata S, Block GD, Colwell CS. Circadian-based Treatment Strategy Effective in the BACHD Mouse Model of Huntington's Disease. *J Biol Rhythms*. 2018 Oct;33(5):535-554. doi: 10.1177/0748730418790401.
- Whittaker DS, Tamai TK, Bains RS, Villanueva SAM, Luk SHC, Dell'Angelica D, Block GD, Ghiani CA, Colwell CS. Dietary ketosis improves circadian dysfunction as well as motor symptoms in the BACHD mouse model of Huntington's disease. *Front Nutr*. 2022; 9:1034743. doi: 10.3389/fnut.2022.1034743.
- Yavuz-Kodat, E., Reynaud, E., Geoffray, M. M., Limousin, N., Franco, P., Bonnet-Brilhault, F., Bourgin, P., & Schroder, C. M. (2020). Disturbances of Continuous Sleep and Circadian Rhythms Account for Behavioral Difficulties in Children with Autism Spectrum Disorder. *Journal of clinical medicine*, 9(6), 1978. <https://doi.org/10.3390/jcm9061978>.
- Yrigollen, C. M., & Davidson, B. L. (2019). CRISPR to the Rescue: Advances in Gene Editing for the FMR1 Gene. *Brain sciences*, 9(1), 17. <https://doi.org/10.3390/brainsci9010017>.
- Yuskaitis, Christopher J., Eleonore Beurel, and Richard S. Jope. "Evidence of reactive astrocytes but not peripheral immune system activation in a mouse model of Fragile X syndrome." *Biochimica et Biophysica Acta (BBA)-Molecular Basis of Disease* 1802.11 (2010): 1006-1012.
- Zalfa, F., Achsel, T., & Bagni, C. (2006). mRNPs, polysomes or granules: FMRP in neuronal protein synthesis. *Current opinion in neurobiology*, 16(3), 265–269. <https://doi.org/10.1016/j.conb.2006.05.010>.
- Zhang J, Fang Z, Jud C, Vansteensel MJ, Kaasik K, Lee CC, Albrecht U, Tamanini F, Meijer JH, Oostra BA, Nelson DL. Fragile X-related proteins regulate mammalian circadian behavioral rhythms. *Am J Hum Genet*. 2008 Jul;83(1):43-52. doi: 10.1016/j.ajhg.2008.06.003.
- Zhang, P. P., Yao, H. H., Zha, A. H., Liu, X. Y., Fan, K. Y., Xu, Y., Yuan, H. Y., Li, L., & Wang, L. C. (2020). Cellular localization of the FMRP in rat retina. *Bioscience reports*, 40(6), BSR20200570. <https://doi.org/10.1042/BSR20200570>

Figure Legends

Fig. 1: The *Fmr1* KO mice exhibited shorter and fragmented sleep in the light phase. (A) Waveforms of daily rhythms in sleep behavior under standard 12:12 h light-dark (LD) cycles in both WT (blue circle) and *Fmr1* KO (yellow triangle) mice ($n = 6/\text{genotype}$). By definition, ZT 0 is when the lights turn on and ZT 12 is when the lights turn off. The sleep waveform (1 hr bins) of each genotype were analyzed using a two-way ANOVA with genotype and time as factors, followed by the Holm-Sidak's multiple comparisons test. Significant differences ($P < 0.05$) are indicated with an asterisk (*). Both genotypes exhibited clear rhythms in sleep, with reductions in the mutants mostly found in the light phase. The white/black bar on the top indicates the LD cycle, and the gray shading in the waveforms indicates the time of the dark phase. **(B-D)** Measures of immobility-defined sleep in the light phase. Values are shown as the means \pm SEM. Genotypic differences were analyzed with a *t*-test and significant differences ($P < 0.05$) are indicated with an asterisk (*). See **Table 1**.

Fig. 2: The *Fmr1* KO mice exhibited unstable locomotor activity rhythms and reduced nocturnality. (A) Representative wheel-running actograms of daily rhythms in cage activity under LD cycles followed by the constant darkness (DD) in both WT (left) and *Fmr1* KO (right) mice. The activity levels in the actograms were normalized to the same scale (85% of the maximum of the most active individual). Each row represents two consecutive days, and the second day is repeated at the beginning of the next row. **(B)** Waveforms of daily rhythms in cage activity in both WT (blue circle) and *Fmr1* KO (yellow triangle) mice under the LD cycles ($n = 6/\text{genotype}$). The activity waveform (1 hr bins) was analyzed using a two-way ANOVA with genotype and time as factors followed by the Holm-Sidak's multiple comparisons test. Significant differences ($P < 0.05$) are indicated with an asterisk (*). There were significant effects of time ($F = 8.84$; $P = 0.003$) and genotype ($F = 39.75$; $P < 0.001$) on the temporal pattern of the locomotor activity rhythms. Note that genotypic differences were found before and after dawn. Measures of locomotor activity rhythm parameters under LD **(C)** and DD **(D)**. Histograms show the means \pm SEM with the values from individual animals overlaid, and the genotypic differences were analyzed by a *t*-test ($*P < 0.05$). The white/black bars on the top of the actograms and waveforms indicate the LD cycle, and the gray shading in the waveforms indicates the time of dark exposure. See **Table 2**.

Fig. 3: The *Fmr1* KO mice showed deficits in light-regulated circadian behaviors. (A, B) Photic-suppression (masking) of activity in mice exposed to light at 300 lx (4500K) for an hour at ZT 14 ($n=10/\text{genotype}$). The activity level during the light exposure was compared to the activity level during the equivalent hour (ZT 14-15) on the day before the treatment (baseline activity). **(A)** The genotypic difference in the fold change was determined by *t*-test, with the mutants showing significantly lower suppression of activity as compared to the WT ($*P = 0.05$). **(B)** The changes in activity levels of the individual mice during the baseline window and the light masking were analyzed using the paired *t*-test in WT ($P < 0.001$) and *Fmr1* KO ($P = 0.12$). **(C, D)** Entrainment induced by a 6 hr-phase advanced LD cycle. Examples of light-induced phase shifts of wheel-running activity rhythms **(C)** of a WT (left) and an *Fmr1* KO (right) are shown. The white/black bars on the top of actograms indicate the LD cycle before (upper) and after (lower) the 6 hr phase advance. The gray shading in the waveforms indicates the time of dark phase. The arrows next to the actograms indicate the day when the 6 hr-phase advance was applied. Two-way ANOVA confirmed significant effects of genotype ($F_{(1, 285)} = 130.157$, $P < 0.001$). The entrainment shifting in the WT (blue circle) and the *Fmr1* KO (yellow triangle) is quantified by the difference between the activity onset and the new ZT12 on each day **(D)**. The arrow heads indicate the day when the activity rhythms are considered well entrained. The *Fmr1* KO took significantly longer to re-entrain to the new LD cycle ($P < 0.001$). See **Table 3**.

Fig. 4: The *Fmr1* KO mice exhibited difficulty in adapting to the skeleton photic period (SPP). (A) Representative actograms of daily rhythms in cage activity under standard LD cycles followed by the SPP challenge (1hr:11hr:1hr:11hr LD cycles) in both WT (left) and *Fmr1* KO (right) mice. The white/black bars on the top of actograms indicate the baseline LD cycle (upper) and the SPP LD cycles (lower). The gray shading in the waveforms indicates the time of the dark phase. **(B)** Measures of locomotor activity rhythms under the SPP environment. Many of the parameters measured were significantly different between the genotypes. Histograms show means \pm SEM with the values from individual animals overlaid. Significant differences ($P < 0.05$) by *t*-test or Mann-Whitney Rank sum test are indicated with an asterisk (*). See **Table 3. (C,D)** Light-

induced phase delay of free-running activity rhythms in mice exposed to light (300 lx, 4500K, 15 mins) at circadian time (CT) 16. By definition, CT 12 is the beginning of the activity cycle under DD conditions for a nocturnal organism. Examples of light-induced phase shifts of wheel-running activity rhythms (**C**) of WT (left) and *Fmr1* KO (right) and quantified phase delay (**D**) ($n = 7/\text{group}$). In the representative actograms, the yellow lines indicate the best-fit line of the activity onset across the 10 days before and after the light pulse. The amount of the phase delay is determined by the difference between the two lines on the next day after the light pulse. The sunny-shape symbols indicate when the mice were exposed to light (CT16). Compared to WT, the *Fmr1* KO showed reduced phase shift of their activity rhythms (Mann Whitney $U^*P = 0.011$). See **Table 3**.

Fig. 5: Abnormal Retinal-Suprachiasmatic Nucleus connectivity in the *Fmr1* KO mice. To trace the projections from the retina to the suprachiasmatic nucleus (SCN) via the Retino-Hypothalamic tract (RHT), WT and *Fmr1* KO mice received a bilateral intravitreal injection of Cholera Toxin (β -subunit) conjugated to Alexa Fluor555 and were perfused 72 hours later. (**A**) Lower intensity of the Cholera Toxin fluorescently labelled RHT projections can be observed both laterally and medially to the ventral part of the SCN in the *Fmr1* KO mice as compared to WT, suggesting a loss of afferent projections to the SCN. (**B, C**) Densitometric analysis of the distribution of the cholera toxin fluorescence intensity in the ventral SCN (**Suppl. Fig. 1**) of WT and *Fmr1* KO mice. The intensity peaks of the profile plot of 4 to 5 consecutive coronal sections containing the middle SCN were aligned and then averaged to obtain a single curve per animal. Results are shown as the mean \pm standard deviation (SD) for the left (**B**) and the right (**C**) SCN of 3 animals per genotype. (**D, E**) cFos-induction was greatly reduced in the SCN of the *Fmr1* KO mice compared to WT. Mice held in DD, were exposed to light (300 lx, 4500K) pulse for 15 min at CT 16, then perfused 45 minutes later (CT 17). (**D**) Representative serial images of light-evoked cFos expression in the SCN. The inset in the lower left panel shows the lack of cFos immunopositive cells in the SCN of mice held in DD but not exposed to the light pulse. (**E**) The number of immune-positive cells in the left and right SCN from 3-5 consecutive coronal sections per animal were averaged to obtain one number per animal and are presented as the mean \pm SD of 4 animals per genotype. One-way ANOVA followed by Bonferroni's multiple comparisons test, $*P=0.0201$. See **Table 4**

Fig. 6: The deficits in social recognition and repetitive behaviors of the *Fmr1* KO mice correlate with sleep behavior. Social behavior was evaluated with the 3-chamber social test. (**A**) In the first stage, the testing mouse was given a choice between a novel mouse and an inanimate object. The social preference index (SPI) was determined. WT mice preferred to spend time with a novel mouse compared to the *Fmr1* KO and had a higher SPI. (**B**) In the second stage of the 3-chamber test, the testing mouse was given the choice between a chamber with a novel mouse and one with the familiar mouse. The social novelty preference index (SNPI) was determined. WT mice preferred to spend time with the novel mouse compared to the familiar one and had a higher SNPI compared to the *Fmr1* KO. (**C**) The possibility of impaired social memory was further tested by the 5-trial social test. In this test, the first stranger mouse becomes a familiar mouse after 4 exposures to the testing mouse. When a novel mouse is introduced in the 5th trial, the WT mice showed a higher interest in the novel mouse compared to *Fmr1* KO mice. Test of repetitive behaviors were also performed. With the marble bury test, the amount of digging in the bedding (**D**) and the percentage of marbles buried (**E**) were measured. *Fmr1* KO mice spent longer time digging and buried more marbles compared to WT. Grooming behaviour, assessed in a novel arena, was significantly higher in the *Fmr1* KO mice as compared to WT. Histograms show the means \pm SEM with the values from individual animals overlaid. Significant differences ($P < 0.05$) by t -test or Mann-Whitney Rank sum test are indicated with an asterisk (*). See **Table 4**. (**G-J**) Sleep duration (**G, H**) and sleep fragmentation (**I, J**) were correlated with social recognition and grooming behaviors (Pearson Correlation test). See **Table 5**.

Fig. 7: Amelioration of sleep/wake rhythms in the *Fmr1* KO mutants by TRF. (**A, B**) Waveforms of daily rhythms in cage activity (IR detection) in the WT (circle) and *Fmr1* KO (triangle) mice under the *ad lib* feeding (ALF) or the TRF (filled) feeding paradigms ($n = 8/\text{group}$). The activity waveforms (1 hr bins) were analyzed using a three-way ANOVA with genotype, treatments, and time as factors followed by Holm-Sidak's multiple comparisons test. There were significant effects of genotype ($F_{(1, 767)} = 13.301$; $P < 0.001$) and time ($F_{(23, 767)} = 94.188$; $P < 0.001$), as well as significant interactions between genotype and time ($P < 0.001$) and treatment and time ($P < 0.001$) on the locomotor activity rhythms of WT and *Fmr1* KO mice. (**C-E**) Measures of locomotor activity rhythms. Both genotypes exhibited an increase in rhythm power under TRF compared to ALF controls. The increase in early day activity and cycle-to-cycle variation seen in the *Fmr1* KO mice was

corrected by TRF. Data are shown as the means \pm SEM; two-way ANOVA followed by Holm-Sidak's multiple comparisons test with genotype and diet as factors, * $P < 0.05$ significant differences between diet regimens; # $P < 0.05$ significant differences between genotypes. See also **Table 6. (F, G)** Waveforms of daily rhythms in the immobility-defined sleep. The sleep waveform (1 hr bins) was analyzed using a two-way ANOVA with time and the feeding treatments as factors followed by Holm-Sidak's multiple comparisons test. There were significant effects of time for both WT ($F_{(23, 351)} = 9.828, P < 0.001$) and *Fmr1* KO ($F_{(23, 351)} = 1.806, P = 0.014$) mice. Treatment did not significantly affect either genotype. Missing data points precluded the use of three-way ANOVA for measures. **(H-J)** Measures of immobility-defined sleep in the light phase. Both genotypes held on TRF exhibited an increase in sleep duration and in sleep bout duration as well as a reduction in sleep fragmentation compared to ALF controls. Data are shown as the means \pm SEM; two-way ANOVA followed by Holm-Sidak's multiple comparisons test with genotype and diet as factors, * $P < 0.05$ significant differences between diet regimens; # $P < 0.05$ significant differences between genotypes. See **Table 6**.

Fig. 8: TRF improved social memory and stereotypic grooming behavior in the *Fmr1* KO mice. (A) Social memory was evaluated by the 5-trial social interaction test as described above. The social memory of the *Fmr1* KO was significantly increased by the TRF intervention, suggesting that the treated mutants were able to distinguish the novel mouse from the familiar mouse. The left panels show the time spent in social interactions when the second novel stranger mouse was introduced to the testing mouse in the 5-trial social interaction test. The significant differences were analyzed by two-way ANOVA followed by the Holm-Sidak's multiple comparisons test with the feeding treatments and genotype as factors. * $P < 0.05$ indicates the significant time spent with novel mouse compared to familiar mouse. Note that the *Fmr1* KO under ALF exhibited a slight preference for the novel mouse while under TRF this preference was higher. **(B)** Grooming was assessed in a novel arena in mice of each genotype (WT, *Fmr1* KO) under each feeding condition and the resulting data analyzed by two-way ANOVA followed by the Holm-Sidak's multiple comparisons test with feeding treatment and genotype as factors. * $P < 0.05$ indicates the significant difference between the feeding treatments, and # $P < 0.05$ indicates the significant difference between the genotypes. **(C)** Distance travelled in the grooming test. TRF did not alter the overall locomotion in the treated mice. See **Table 7**.

Fig. 9: The plasma levels of IL-12 and IFN γ correlate with altered sleep/wake rhythms and autistic behaviors, and are corrected by TRF in the *Fmr1* KO mice. (A) The levels of selected plasma pro-inflammatory markers are shown. The full list of assayed makers is reported in **Table 8** (n=8/group). Data were analyzed with two-way ANOVA followed by the Holm-Sidak's multiple comparisons test with treatment and genotype as factors. * $P < 0.05$ indicates the significant difference between the feeding treatments, and # $P < 0.05$ indicates the significant difference between the genotypes. **(B-G)** Correlations between IL-12/IFN- γ and sleep time, social recognition, and grooming behavior. Data were analyzed using the Pearson Correlation, and the coefficients are reported in **Table 9**.

Supplementary Figure 1: The distribution of the Cholera Toxin fluorescent signal was obtained for each left and right SCN using the Profile Plot Analysis feature of ImageJ. A rectangular box of fixed size (415.38 μ m x 110.94 μ m, width x height) was created to include the entire ventral part of the SCN. A column plot profile was generated whereby the x-axis represents the horizontal distance through the SCN (lateral to medial for the left SCN and medial to lateral for the right SCN; as indicated by the arrows) and the y-axis represents the average pixel intensity per vertical line within the rectangular box.

Supplementary Figure 2: (A) Food consumption of WT and *Fmr1* KO mice under ALF or TRF. Over the two weeks of scheduled feeding, no significant differences were found in the total amount of food consumed between the genotypes ($F_{(1, 31)} = 3.086, P = 0.090$) or with feeding schedule ($F_{(1, 31)} = 0.307, P = 0.584$). If we just analyzed the food consumed over the first three days, there were no effects of genotype ($F_{(1, 31)} = 2.737, P = 0.109$) but the TRF groups consumed less ($F_{(1, 31)} = 85.912, P < 0.001$). **(B)** Under baseline conditions, the mice had similar weights (WT: 22.1 \pm 0.4 g; KO: 23.1 \pm 0.4 g; $t_{(30)} = -1.748, P = 0.090$). After two weeks, the TRF treated mice exhibited lower weights than those on ALF ($F = 30.551; P < 0.001$). The Holm-Sidak's multiple comparisons test indicated that both WT and *Fmr1* KO mice exhibited reduced weights ($P < 0.01$) after TRF.

Table 1: Altered behavioral sleep parameters in the *Fmr1* KO mice. Comparisons of sleep behavior in age-matched male WT and *Fmr1* KO mice (n = 6/group). Values are shown as averages \pm SEM. For the 24-hr data set, values were analyzed using a t-test. Possible day/night differences were analyzed with two-way ANOVA using genotype (WT vs. *Fmr1* KO) and time (day vs. night) as factors, followed by the Holm-Sidak's multiple comparisons test. Asterisks indicate significant differences between the genotypes, while crosshatch significant differences between day and night. Alpha = 0.05. Degrees of freedom are reported between parentheses. Bold values indicate statistically significant differences.

24 hour totals		WT		<i>Fmr1</i> KO		t test	
Sleep duration (min)		645.1 \pm 30.2		568.6 \pm 29.8		$t_{(10)}=1.973$; P=0.077	
Sleep bouts (#)		49.9 \pm 2.7		50.3 \pm 2.0		$t_{(10)}=-0.136$; P=0.895	
Bout duration (min)		15.7 \pm 1.1		13.1 \pm 0.6*		$t_{(10)}=2.329$; P=0.042	
Max bout duration (min)		55.9 \pm 3.8		48.3 \pm 2.7		$t_{(10)}=1.764$; P=0.112	

Measures	WT		<i>Fmr1</i> KO		Two-way Anova		
	Day	Night	Day	Night	Genotype	Time	Interaction
Sleep Duration (min)	464 \pm 19.4[#]	182 \pm 13.5	414 \pm 14.8^{**}	154.6 \pm 17.7	F_(1,23)=6.37; P=0.02	F_(1,23)=319.5; P<0.001	F _(1,23) =0.56; P=0.46
Bout counts (#)	24.4 \pm 1.8	25.5 \pm 2.1	29.6 \pm 1.2^{**}	20.7 \pm 1.9	F _(1,23) =0.017; P=0.90	F_(1,23)=5.70; P=0.027	F_(1,23)=9.33; P=0.006
Bout duration (min)	22.4 \pm 1.9[#]	9.0 \pm 0.7	16.6 \pm 0.8^{**}	9.5 \pm 0.6	F_(1,23)=6.77; P=0.017	F_(1,23)=100.9; P<0.001	F_(1,23)=9.64; P=0.006
Max bout duration (min)	81.3 \pm 6.0[#]	30.5 \pm 3.0	58 \pm 3.09^{**}	38.7 \pm 3.8	F _(1,23) =4.02; P=0.059	F_(1,23)=85.96; P<0.001	F_(1,23)=17.33; P<0.001

Table 2: Activity rhythms were altered in the *Fmr1* KO mutants. The locomotor activity rhythms of adult male WT and *Fmr1* KO mice in the standard 12 h:12 hr LD cycles and constant darkness (DD) were monitored using wheel running activity (n=6/group). Values are shown as averages \pm SEM. If the assumptions of normality and equal variance were met, a *t*-test was used to analyze the data, otherwise the Mann-Whitney Rank sum test was used. Asterisks indicate significant differences between genotypes. Alpha = 0.05. Degrees of freedom are reported between parentheses. Bold values indicate statistically significant differences.

	WT	<i>Fmr1</i> KO	Statistical Values
LD			
Power (% variance)	42.8 \pm 1.7	30.4 \pm 3.8*	$t_{(10)}=3.309$; P=0.008
Cage Activity (rev)	19875 \pm 2197	24302 \pm 4294	$t_{(10)}=-1.005$; P=0.340
Amplitude (rev)	2553 \pm 246	2771 \pm 406	$t_{(10)}=-0.502$; P=0.630
Activity in the Light Phase (ZT 0-3, rev)	418 \pm 50.7	1099 \pm 165*	U=0.000; P=0.002
Cycle-to-cycle variability (min)	8.1 \pm 2.0	24.5 \pm 10.6	$t_{(10)}=-2.060$; P=0.066
Fragmentation (# bouts)	21.0 \pm 0.6	24.2 \pm 2.5	U=12.000; P=0.390
DD			
Tau (h)	23.6 \pm 0.1	23.4 \pm 0.2	$t_{(10)}=0.919$; P=0.380
Power (% variance)	47.4 \pm 1.2	39.1 \pm 2.0*	$t_{(10)}=5.319$; P=0.003
Cage Activity (rev)	27225 \pm 1495	27914 \pm 3218	$t_{(10)}=-0.213$; P=0.836
Onset variability (min)	16.3 \pm 2.9	42.5 \pm 7.9*	$t_{(10)}=-3.387$; P=0.007
Fragmentation (# bouts)	21.3 \pm 1.2	24.1 \pm 1.8	$t_{(10)}=-1.416$; P=0.187

Table 3. Deficits in circadian light response in the *Fmr1* KO mice. The circadian light response of male adult WT and *Fmr1* KO mice was evaluated using four behavioral assays and wheel-running activity. First, masking or the suppression of activity that occurs when mice are exposed to 1-hr of light during the night at ZT 14. Second, the number of days required for the activity rhythms to re-synchronize to a 6 hr advance of the LD cycle. Third, to measure the magnitude of a light-evoked phase shift of the circadian system, mice were held in constant dark (DD) and exposed to light for 15 min at CT 16. Fourth, the mice were held in a skeleton photoperiod (1hr:11hr) and basic locomotor activity parameters were measured. Values are shown as averages \pm SEM. If the assumptions of normality and equal variance were met, a *t*-test was used to analyze the data. If not, a Mann-Whitney Rank sum test was used. Significant differences between the genotypes are shown in bold. Alpha = 0.05. Degrees of freedom are reported between parentheses. Bold values indicate statistically significant differences.

	WT	<i>Fmr1</i> KO	Stats
Masking (% suppression)	77.7 \pm 5.8	32.5 \pm 10.0*	$t_{(18)}=4.131$; P=0.006
Re-entrainment (days)	5.9 \pm 0.6	11.3 \pm 0.4*	$t_{(20)}=-6.868$; P<0.001
Skeleton Photo Period (SPP)			
Period (h)	24.0 \pm 0.0	23.7 \pm 0.2*	U=10.500; P=0.021
Power (% variance)	39.4 \pm 2.0	24.0 \pm 1.6*	$t_{(14)}=6.112$; P<0.001
Cage Activity (rev)	21711 \pm 1662	25257 \pm 2954	$t_{(14)}=-1.119$; P=0.282
Activity in the subjective day (%)	5.29 \pm 1.5	34.7 \pm 6.0*	U=0.000; P<0.001
Onset variability (min)	18.1 \pm 2.8	59.5 \pm 9.1*	$t_{(14)}=-4.668$; P<0.001
Light-evoked phase shift (min)	-135.6 \pm 26.9	-64.0 \pm 7.7*	U=5.500; P=0.011

Table 4. Subtle decrease in the relative intensity of Cholera Toxin (β subunit) in the retinal afferents to the suprachiasmatic nucleus (SCN) of *Fmr1* KO mice. There was a stronger impact of the loss of FMRP on the induction of light-evoked cFos expression in the SCN. Control no pulse= WT mice held in DD but did not receive the light pulse at CT16. Histomorphometrical analysis of the SCN revealed no differences between wild-type and *Fmr1* male mice. All measurements were performed by two independent observers masked to the experimental groups. Results are shown as the mean \pm SD. Alpha = 0.05. Degrees of freedom are reported between parentheses. Bold values indicate statistically significant differences.

Cholera Toxin	WT (n=3)	<i>Fmr1</i> KO (n=3)	Mann-Whitney Test
Mean Intensity (a.u.)	247.2 \pm 52.8	221.8 \pm 29.5	$U = 2; P = 0.4000$
cFos immunopositive cells (#)	WT (n=4)	<i>Fmr1</i> KO (n=4)	Control no pulse (n=3)
One-Way Anova	105.9 \pm 27.5	52.96 \pm 19.4* $F_{(2,8)}=19.75; P=0.0008$	7.720 \pm 1.28
	WT (n=6)	<i>Fmr1</i> KO (n=6)	Mann-Whitney Test
Area (μm^2)	308184 \pm 6198	294721 \pm 11561	$U = 11; P = 0.3095$
Perimeter (μm)	1178 \pm 40.84	1154 \pm 60.82	$U = 11; P = 0.3095$
Height (μm)	395.2 \pm 21.69	386.9 \pm 20.13	$U = 11; P = 0.3095$
Width (μm)	338.1 \pm 16.05	333.7 \pm 24.08	$U = 12; P = 0.3939$

Table 5. *Fmr1* KO mutants present with deficits in social discrimination. Comparisons of social discrimination behavior in age-matched WT and *Fmr1* KO mice (n = 8/group) were assessed using the 3-chamber and the 5-trial social interaction test. Social Preference Index (SPI) = difference in the time spent with the novel mouse and object divided by the sum of the time spent with the novel mouse and the object. Social Novelty Preference Index (SNPI) = difference in the time spent with the novel and familiar mouse divided by the sum of the time spent both novel and familiar mice. The repetitive behavior in WT and *Fmr1* KO mice (n=14/genotype) assessed using the marble bury and grooming tests. Values are shown as averages \pm SEM. If the assumptions of normality and equal variance were met, a *t*-test was used to analyze the data, otherwise, the Mann-Whitney test. Alpha = 0.05. Degrees of freedom are reported between parentheses. Bold values indicate statistically significant differences.

	WT	<i>Fmr1</i> KO	Statistical Values
3-chamber social test			
Time with object (sec)	154 \pm 7.4	184 \pm 13.3	$t_{(14)}=-2.100$; P=0.054
Time with mouse (sec)	236 \pm 13.6	210 \pm 14.5	$t_{(14)}=1.777$; P=0.097
SPI	0.20 \pm 0.04	0.06 \pm 0.05*	U=12.500 ; P=0.038
3-chamber social recognition test			
Familiar-mouse chamber (sec)	143 \pm 11.2	173 \pm 1.7*	U=11.000 ; P=0.028
Novel-mouse chamber (sec)	225 \pm 13.5	209.5 \pm 14.2	$t_{(14)}=0.879$; P=0.394
SNPI	0.22 \pm 0.04	0.09 \pm 0.04*	$t_{(14)}=2.445$; P=0.028
5-trial social recognition test			
Familiar mouse (trial 1-4, sec)	154 \pm 15.3	150 \pm 20.9	$t_{(14)}=0.153$; P=0.881
Novel mouse (trial 5, sec)	46.7 \pm 2.8	25.9 \pm 4.7*	$t_{(14)}=3.781$; P=0.002
Marble Bury Test			
Digging in total of 30 mins (sec)	19.8 \pm 4.2	106 \pm 28.0*	U=30.000 ; P=0.002
Buried Marbles (%)	19.6 \pm 6.1	45.8 \pm 8.6*	$t_{(26)}=-2.255$; P=0.017
Distance Travelled (m)	49.1 \pm 3.5	63.9 \pm 2.7*	$t_{(26)}=-3.497$; P=0.002
Grooming Test			
Grooming (sec)	25.5 \pm 2.3	54.4 \pm 4.3*	U=13.000 ; P<0.001
Distance Travelled (m)	67.7 \pm 2.6	78.0 \pm 2.4*	$t_{(26)}=-2.985$; P=0.006

Table 6. Correlation between sleep disturbances in the *Fmr1* KO mice and the severity of impaired behaviors. Data obtained from age-matched WT and *Fmr1* KO mice housed under standard LD cycles were tested for associations with the Pearson Correlation test. The most prominent sleep phenotypes are usually observed during the animals light-phase sleep, hence, only measures between ZT 0-12 were used for these analyses. The correlation coefficients are reported, those significant are shown in bold and labeled with an asterisk. Alpha = 0.05.

	3-chamber social test (SNPI)	Social recognition (trial 5, sec)	Digging (sec)	Marble Buried (%)	Grooming (sec)
Rhythmic Strength (V%)	0.18	0.43	0.13	-0.051	-0.62*
Onset variability (min)	-0.37	-0.4	0.23	0.61*	0.63*
Sleep (min)	0.47	0.86*	-0.3	-0.52	-0.8*
Sleep Bout Counts (#)	-0.39	-0.53	0.27	0.78*	0.7*
Avg. Sleep Bout Length (min)	0.44	0.59*	-0.29	-0.71*	-0.75*
MAX Sleep Bout Length (min)	0.49	0.76*	-0.4	-0.65*	-0.78*

Table 7. Scheduled Feeding improved sleep/wake rhythms in the *Fmr1* KO mutants. Locomotor activity rhythms and immobility-defined sleep were recorded from WT and *Fmr1* KO mice on *ad libitum* feeding (ALF) or time-restricted feeding (TRF) regimen (n=8/genotype/treatment). As the running wheels interfered with our feeders, we used IR to measure the activity rhythms in these experiments. Since the most prominent sleep phenotypes are observed during their light-phase sleep and sleep recordings were paused during the dark phase for adding (ZT15) and removing (ZT21) food, the analyses below only focused on the effects of TRF on sleep during the light-phase sleep (ZT 0-12). Values are shown as averages \pm SEM. Data were analyzed by two-way ANOVA with genotype and treatment as factors, followed by the Holm-Sidak's multiple comparisons test. Asterisks indicate significant differences between diet regimen, while crosshatch significant differences between genotypes. Alpha = 0.05. Degrees of freedom are reported between parentheses. Bold values indicate statistically significant differences.

Activity Rhythms	WT		<i>Fmr1</i> KO		2-way ANOVA		
	ALF	TRF	ALF	TRF	Genotype	Treatment	Interaction
Power (% variance)	41.8 \pm 3.8	50.9 \pm 3.1*	33.2 \pm 3.8	51.1 \pm 2.2*	$F_{(1, 31)}=1.9; P=0.18$	$F_{(1, 31)}=19.41; P<0.001$	$F_{(1, 31)}=2.04; P=0.17$
Cage Activity (a.u.)	4307 \pm 517	4064 \pm 396	3748 \pm 402	3750 \pm 471	$F_{(1, 31)}=1.08; P=0.31$	$F_{(1, 31)}=0.082; P=0.78$	$F_{(1, 31)}=0.085; P=0.77$
Light-Phase Activity (ZT 0-3, a.u.)	255 \pm 18.9	194 \pm 24.3	443 \pm 59.6 [#]	246 \pm 42.0*	$F_{(1, 31)}=10.44; P=0.03$	$F_{(1, 31)}=12.14; P=0.002$	$F_{(1, 31)}=3.38; P=0.07$
Onset variability (min)	6.8 \pm 1.6	9.4 \pm 1.3	38.5 \pm 7.5 [#]	6.8 \pm 0.9*	$F_{(1, 31)}=15.58; P<0.001$	$F_{(1, 31)}=15.70; P<0.001$	$F_{(1, 31)}=21.68; P<0.001$
Fragmentation (# bouts)	29.3 \pm 1.7	23.4 \pm 1.0*	29.5 \pm 1.8	23.4 \pm 1.1*	$F_{(1, 31)}=0.11; P=0.74$	$F_{(1, 31)}=21.91; P<0.001$	$F_{(1, 31)}=0.23; P=0.64$
Sleep							
Total Sleep (min)	414 \pm 6.3	525 \pm 11.9*	384 \pm 7.4 [#]	481 \pm 15.7**	$F_{(1, 31)}=18.35; P<0.001$	$F_{(1, 31)}=127.19; P<0.001$	$F_{(1, 31)}=0.96; P=0.34$
Sleep Bouts (#)	20.2 \pm 1.3	12.7 \pm 0.8*	21.4 \pm 1.1	15.4 \pm 0.9*	$F_{(1, 31)}=4.21; P=0.05$	$F_{(1, 31)}=47.94; P<0.001$	$F_{(1, 31)}=0.59; P=0.45$
Avg. Bout Length (min)	24.6 \pm 1.7	47.0 \pm 3.2*	21.7 \pm 1.04	35.3 \pm 2.7**	$F_{(1, 31)}=11.04; P=0.002$	$F_{(1, 31)}=68.3; P<0.001$	$F_{(1, 31)}=4.03; P=0.055$
MAX Bout Length (min)	96.4 \pm 4.3	137 \pm 3.3*	88.3 \pm 3.1	109 \pm 4.7**	$F_{(1, 31)}=25.03; P<0.001$	$F_{(1, 31)}=68.76; P<0.001$	$F_{(1, 31)}=7.64; P=0.01$

Table 8. Scheduled Feeding improved social recognition memory and reduced grooming behavior in the *Fmr1* KO mice. Adult male WT and *Fmr1* KO mice on ALF or TRF (n=8/genotype/treatment) were exposed to the 5-trial social test and the grooming test. Values are shown as averages \pm SEM. Data were analyzed by two-way ANOVA with genotype and treatment as factors followed by the Holm-Sidak's multiple comparisons test. Asterisks indicate significant differences between diets, while crosshatch significant differences between genotypes. Alpha = 0.05. Degrees of freedom are reported between parentheses. Bold values indicate statistically significant differences.

Measures	WT		<i>Fmr1</i> KO		Two-Way ANOVA		
	ALF	TRF	ALF	TRF	Genotype	Treatment	Interaction
Familiar mouse (trial 1-4, sec)	80.5 \pm 12	96.5 \pm 14	67.5 \pm 4.7	95.8 \pm 15	$F_{(1, 31)}=0.36$; $P=0.55$	$F_{(1, 31)}=3.77$; $P=0.062$	$F_{(1, 31)}=0.29$; $P=0.59$
Novel mouse (trial 5, sec)	43.8 \pm 8.9	66.1 \pm 8.8	23.3 \pm 4.0 [#]	50.3 \pm 10*	$F_{(1, 31)}=5.37$; $P=0.028$	$F_{(1, 31)}=9.88$; $P=0.004$	$F_{(1, 31)}=0.092$; $P=0.76$
Grooming (sec)	19.9 \pm 1.2	16.9 \pm 2.7	41.4 \pm 1.7[#]	26.2 \pm 3.1^{*#}	$F_{(1, 31)}=60.04$; $P<0.001$	$F_{(1, 31)}=20.74$; $P<0.001$	$F_{(1, 31)}=9.4$; $P=0.005$
Distance Travelled (m)	72.2 \pm 4.2	66.6 \pm 4.7	67.0 \pm 6.6	63.2 \pm 2.2	$F_{(1, 31)}=0.98$; $P=0.33$	$F_{(1, 31)}=1.14$; $P=0.3$	$F_{(1, 31)}=0.039$; $P=0.85$

Table 9. Scheduled feeding affects the levels of plasma cytokine in WT and *Fmr1* KO mice. The level of plasma cytokines was measured in WT and mutants under ALF or TRF regimen (n=8/genotype/treatment). Values are shown as averages \pm SEM. Data were analyzed by two-way ANOVA with genotype and treatment as factors followed by the Holm-Sidak's multiple comparisons test. Asterisks indicate significant differences between diets, while crosshatch significant differences between genotypes. Alpha = 0.05. Degrees of freedom are reported between parentheses. Bold values indicate statistically significant differences.

Measures	WT		<i>Fmr1</i> KO		2-way ANOVA		
	ALF	TRF	ALF	TRF	Genotype	Treatment	Interaction
TNF α	4.1 \pm 1.0	2.6 \pm 0.8	3.9 \pm 0.6	2.5 \pm 1.0	$F_{(1, 31)} = 0.03; P = 0.86$	$F_{(1, 31)} = 3.42; P = 0.075$	$F_{(1, 31)} = 0.009; P = 0.93$
IL-2	1.7 \pm 0.2	1.3 \pm 0.3	2.1 \pm 0.2	1.1 \pm 0.3*	$F_{(1, 31)} = 0.16; P = 0.69$	$F_{(1, 31)} = 11.14; P = 0.002$	$F_{(1, 31)} = 1.83; P = 0.19$
IL-3	0.9 \pm 0.1	0.7 \pm 0.1	1.0 \pm 0.1	0.8 \pm 0.2	$F_{(1, 31)} = 0.32; P = 0.58$	$F_{(1, 31)} = 1.51; P = 0.23$	$F_{(1, 31)} < 0.001; P = 0.98$
IL-5	14.1 \pm 2.1	5.9 \pm 1.1*	12.4 \pm 1.3	8.9 \pm 1.9	$F_{(1, 31)} = 0.17; P = 0.68$	$F_{(1, 31)} = 14.35; P < 0.001$	$F_{(1, 31)} = 2.34; P = 0.14$
IL-6	3.1 \pm 0.5	3.9 \pm 1.3	3.5 \pm 0.6	3.1 \pm 1.0	$F_{(1, 31)} = 0.046; P = 0.83$	$F_{(1, 31)} = 0.023; P = 0.88$	$F_{(1, 31)} = 0.5; P = 0.49$
IL-10	4.8 \pm 1.4	3.9 \pm 1.5	3.4 \pm 0.9	3.9 \pm 1.9	$F_{(1, 31)} = 0.24; P = 0.63$	$F_{(1, 31)} = 0.027; P = 0.87$	$F_{(1, 31)} = 0.25; P = 0.63$
IL-12 (p40)	6.2 \pm 2.3	5.0 \pm 1.7	20.9 \pm 4.0#	5.2 \pm 2.4*	$F_{(1, 31)} = 8.44; P = 0.007$	$F_{(1, 31)} = 10.85; P = 0.003$	$F_{(1, 31)} = 7.97; P = 0.009$
IL-15	40.2 \pm 8.0	62.4 \pm 25.5	49.7 \pm 16.4	48.9 \pm 14.4	$F_{(1, 31)} = 0.016; P = 0.9$	$F_{(1, 31)} = 0.44; P = 0.51$	$F_{(1, 31)} = 0.51; P = 0.48$
IL-17	1.8 \pm 0.4	2.9 \pm 0.8	3.4 \pm 0.5	2.4 \pm 1.0	$F_{(1, 31)} = 0.66; P = 0.42$	$F_{(1, 31)} = 0.0026; P = 0.96$	$F_{(1, 31)} = 2.61; P = 0.12$
CCL-2	17.9 \pm 4.6	12.3 \pm 4.8	9.3 \pm 1.6	11.2 \pm 5.4	$F_{(1, 31)} = 1.42; P = 0.24$	$F_{(1, 31)} = 0.22; P = 0.64$	$F_{(1, 31)} = 0.87; P = 0.36$
CCL-5	7.1 \pm 0.6	6.0 \pm 1.2	7.23 \pm 1.2	5.4 \pm 0.9	$F_{(1, 31)} = 0.05; P = 0.82$	$F_{(1, 31)} = 2.56; P = 0.12$	$F_{(1, 31)} = 0.11; P = 0.74$
IFN- γ	2.6 \pm 0.2	2.9 \pm 0.3	5.4 \pm 0.9#	3.7 \pm 0.6*	$F_{(1, 31)} = 10.97; P = 0.03$	$F_{(1, 31)} = 1.96; P = 0.17$	$F_{(1, 31)} = 3.66; P = 0.066$
CXCL-1	105.6 \pm 17.5	91.0 \pm 33.3	83.9 \pm 14	90.3 \pm 20.2	$F_{(1, 31)} = 0.28; P = 0.6$	$F_{(1, 31)} = 0.038; P = 0.85$	$F_{(1, 31)} = 0.25; P = 0.62$
CXCL-5	368.4 \pm 103.9	357.1 \pm 155.5	346.6 \pm 25.4	181.2 \pm 48.4	$F_{(1, 31)} = 0.67; P = 0.42$	$F_{(1, 31)} = 0.017; P = 0.9$	$F_{(1, 31)} = 0.003; P = 0.96$
CXCL-9	207.4 \pm 54.3	225.9 \pm 53.9	346.6 \pm 25.4#	181.2 \pm 48.4*	$F_{(1, 31)} = 1.15; P = 0.29$	$F_{(1, 31)} = 2.79; P = 0.11$	$F_{(1, 31)} = 4.37; P = 0.046$

Table 10. Correlation of the plasma levels of selected inflammatory markers with the level of sleep disturbances and the severity of behavior deficits. Data from all 4 groups (WT ALF, WT TRF, *Fmr1* KO ALF, *Fmr1* KO TRF) were pooled and the Pearson Correlation was applied. The correlation coefficients are reported, those significant are shown in bold and labeled with an asterisk. Alpha = 0.05.

Measures	IL-12 (p40, pg/ml)	IFN- γ (pg/ml)	CXCL-9 (pg/ml)
Rhythmic Strength (V%)	-0.34	-0.15	0.072
Activity in the Light Phase (ZT 0-3, a.u.)	0.73*	0.59*	0.58
Onset variability (min)	0.19*	0.69	0.01
Sleep (min)	-0.48*	-0.48*	0.34
Sleep Bout Counts (#)	0.26	0.16	-0.16
Avg. Sleep Bout Length (min)	-0.36*	-0.24	0.25
MAX Sleep Bout Length (min)	-0.38*	-0.42*	0.34
Social recognition (trial 5, sec)	-0.41*	-0.14	0.34
Repetitive Behavior (grooming, sec)	0.44*	0.45*	0.26

Fig. 1

bioRxiv preprint doi: <https://doi.org/10.1101/2024.09.16.613343>; this version posted September 16, 2024. The copyright holder for this preprint (which was not certified by peer review) is the author/funder, who has granted bioRxiv a license to display the preprint in perpetuity. It is made available under a [CC-BY-NC-ND 4.0 International license](#).

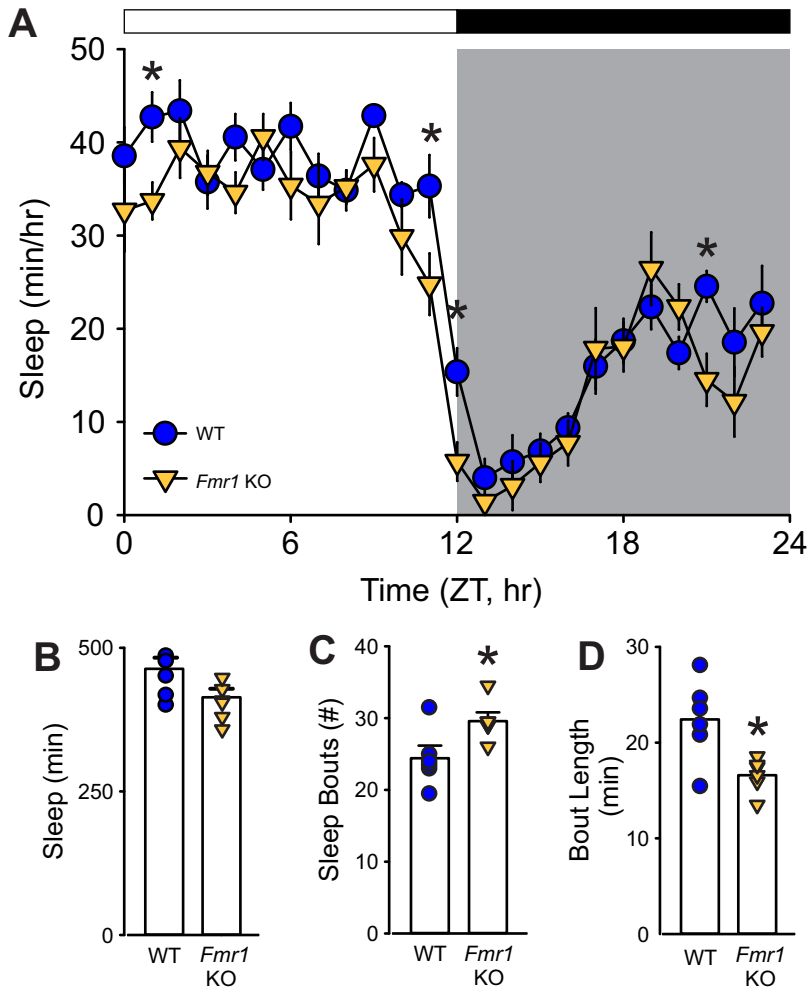


Fig. 2.

bioRxiv preprint doi: <https://doi.org/10.1101/2024.09.16.613343>; this version posted September 16, 2024. The copyright holder for this preprint (which was not certified by peer review) is the author/funder, who has granted bioRxiv a license to display the preprint in perpetuity. It is made available under aCC-BY-NC-ND 4.0 International license.

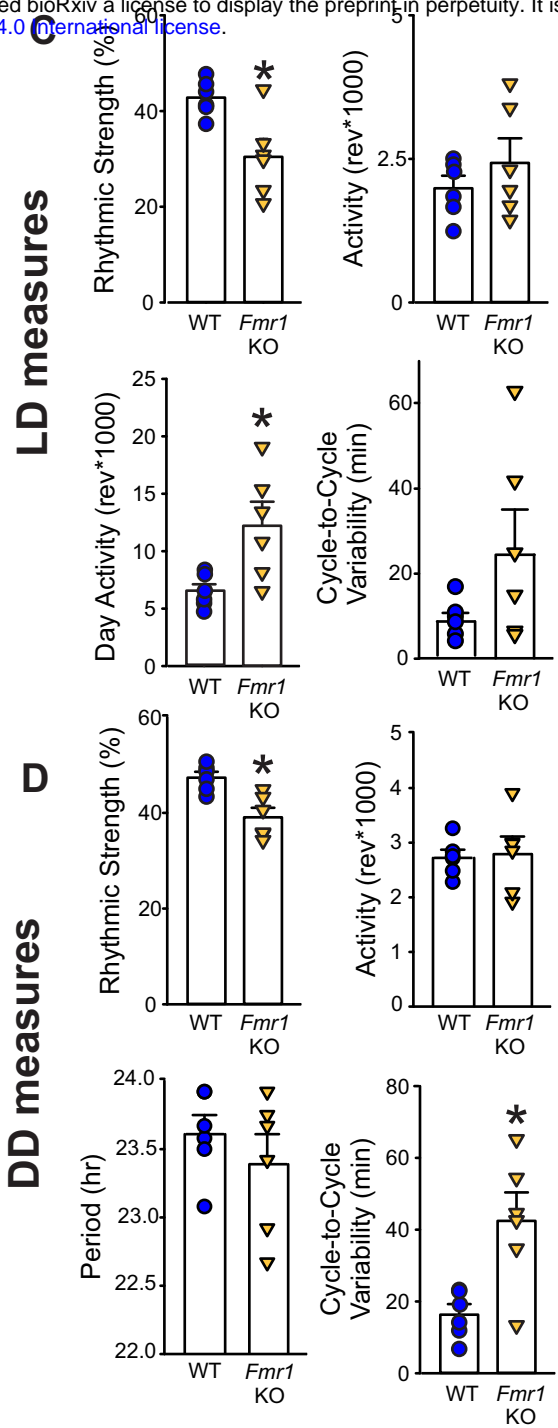
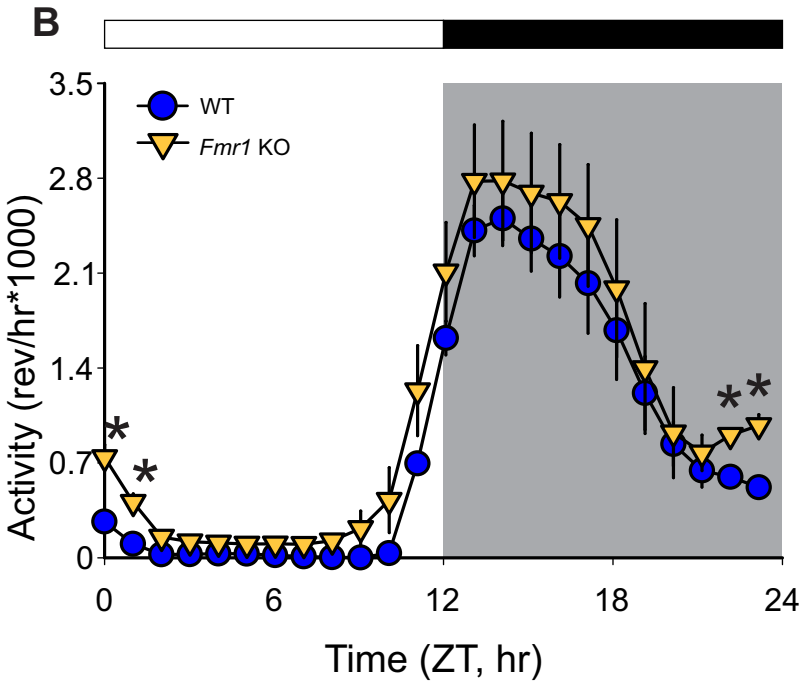
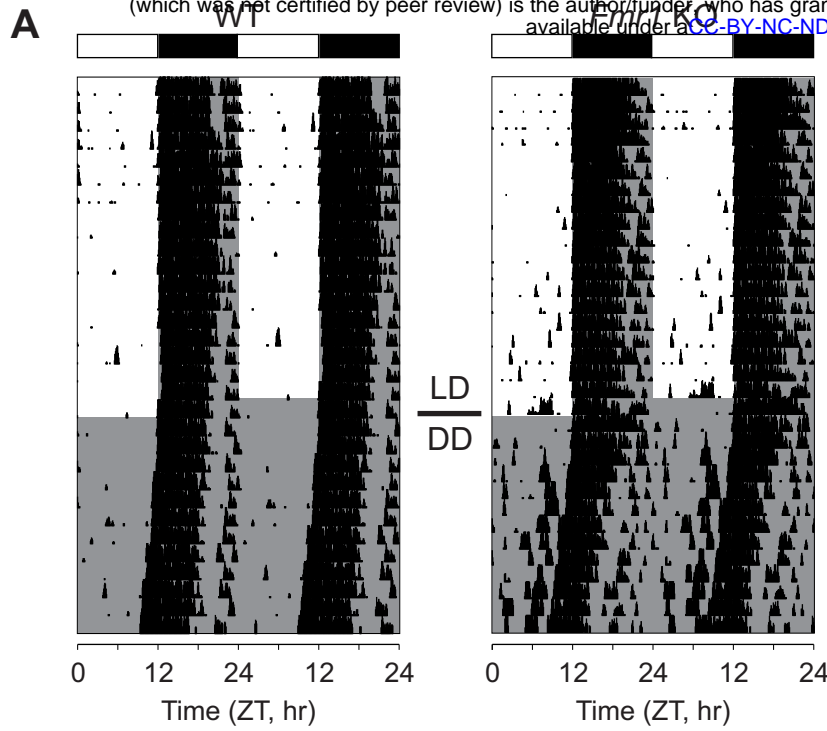


Fig. 3.

bioRxiv preprint doi: <https://doi.org/10.1101/2024.09.16.613343>; this version posted September 16, 2024. The copyright holder for this preprint (which was not certified by peer review) is the author/funder, who has granted bioRxiv a license to display the preprint in perpetuity. It is made available under aCC-BY-NC-ND 4.0 International license.

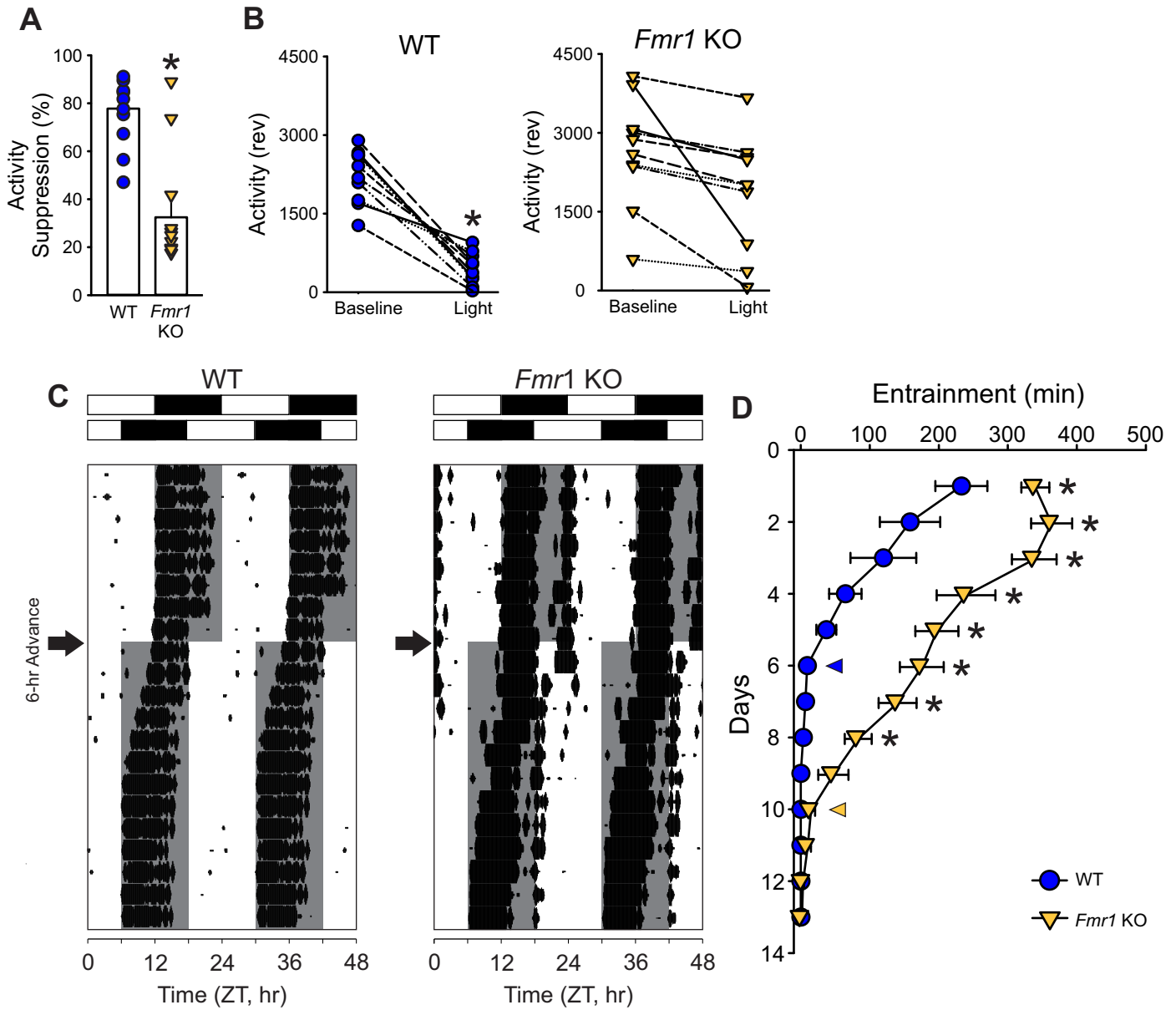


Fig. 4.

bioRxiv preprint doi: <https://doi.org/10.1101/2024.09.16.613343>; this version posted September 16, 2024. The copyright holder for this preprint (which was not certified by peer review) is the author/funder, who has granted bioRxiv a license to display the preprint in perpetuity. It is made available under aCC-BY-NC-ND 4.0 International license.

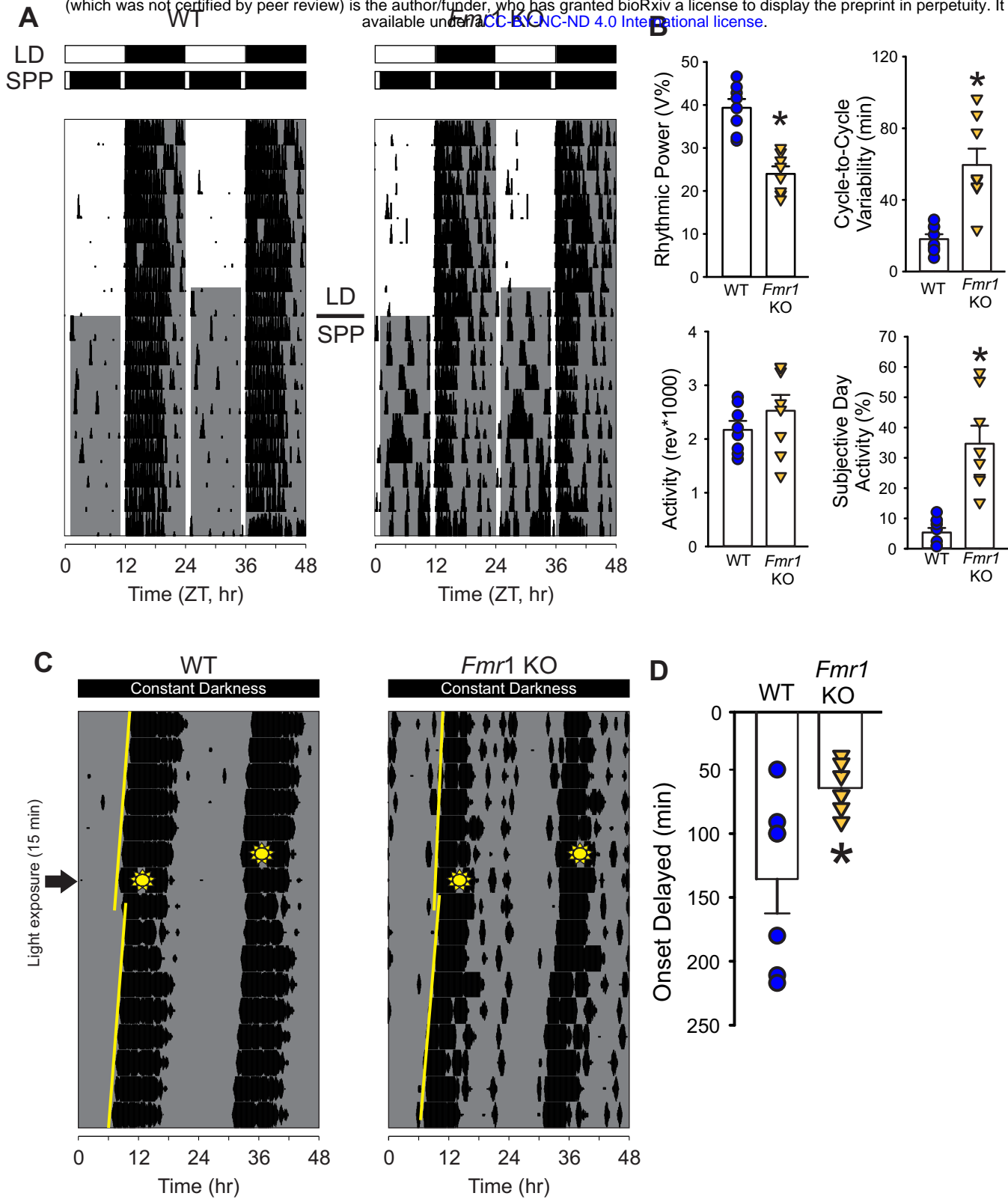


Fig. 5.

bioRxiv preprint doi: <https://doi.org/10.1101/2024.09.16.613343>; this version posted September 16, 2024. The copyright holder for this preprint (which was not certified by peer review) is the author/funder, who has granted bioRxiv a license to display the preprint in perpetuity. It is made available under a [CC-BY-NC-ND 4.0 International license](https://creativecommons.org/licenses/by-nc-nd/4.0/).

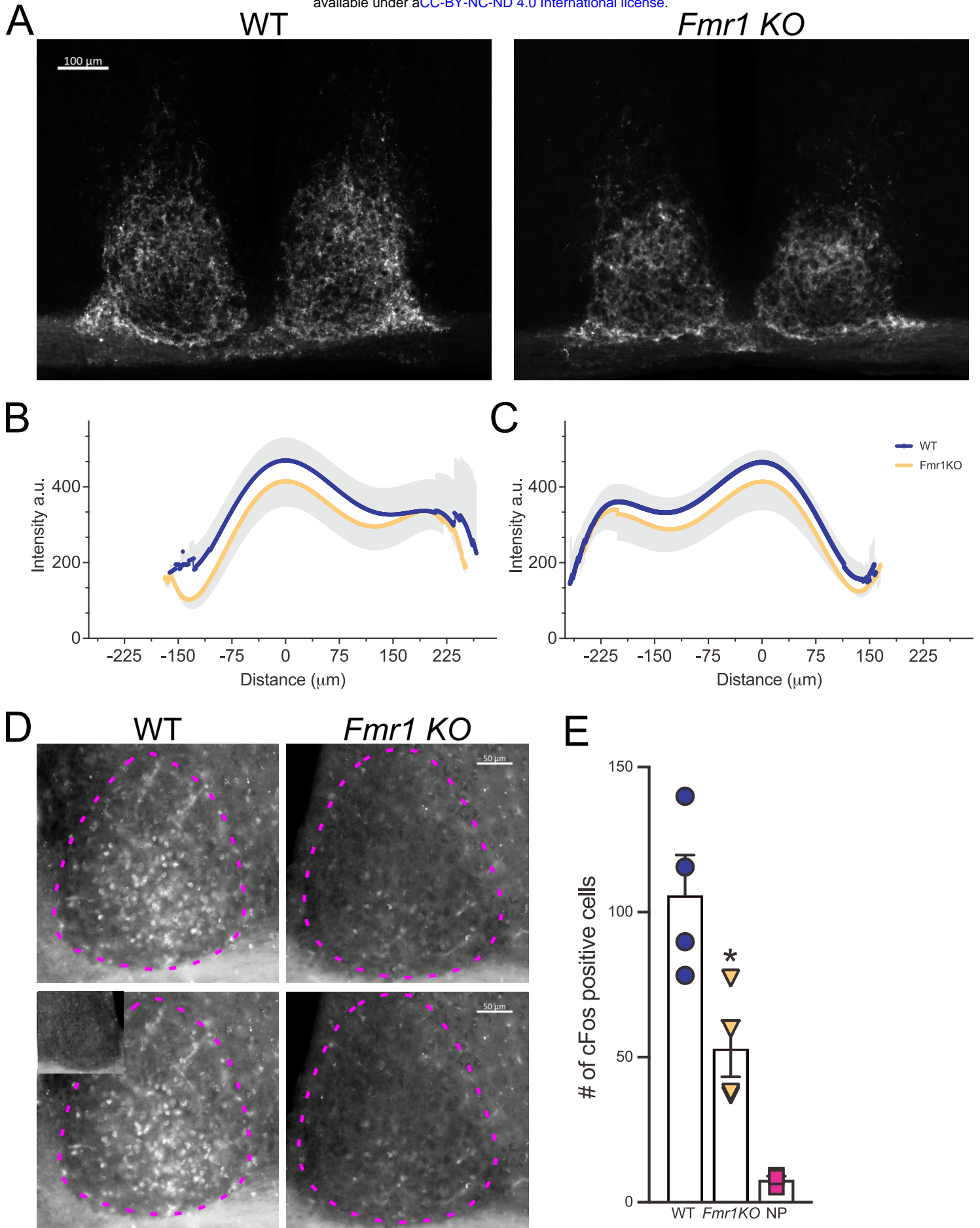


Fig. 6.

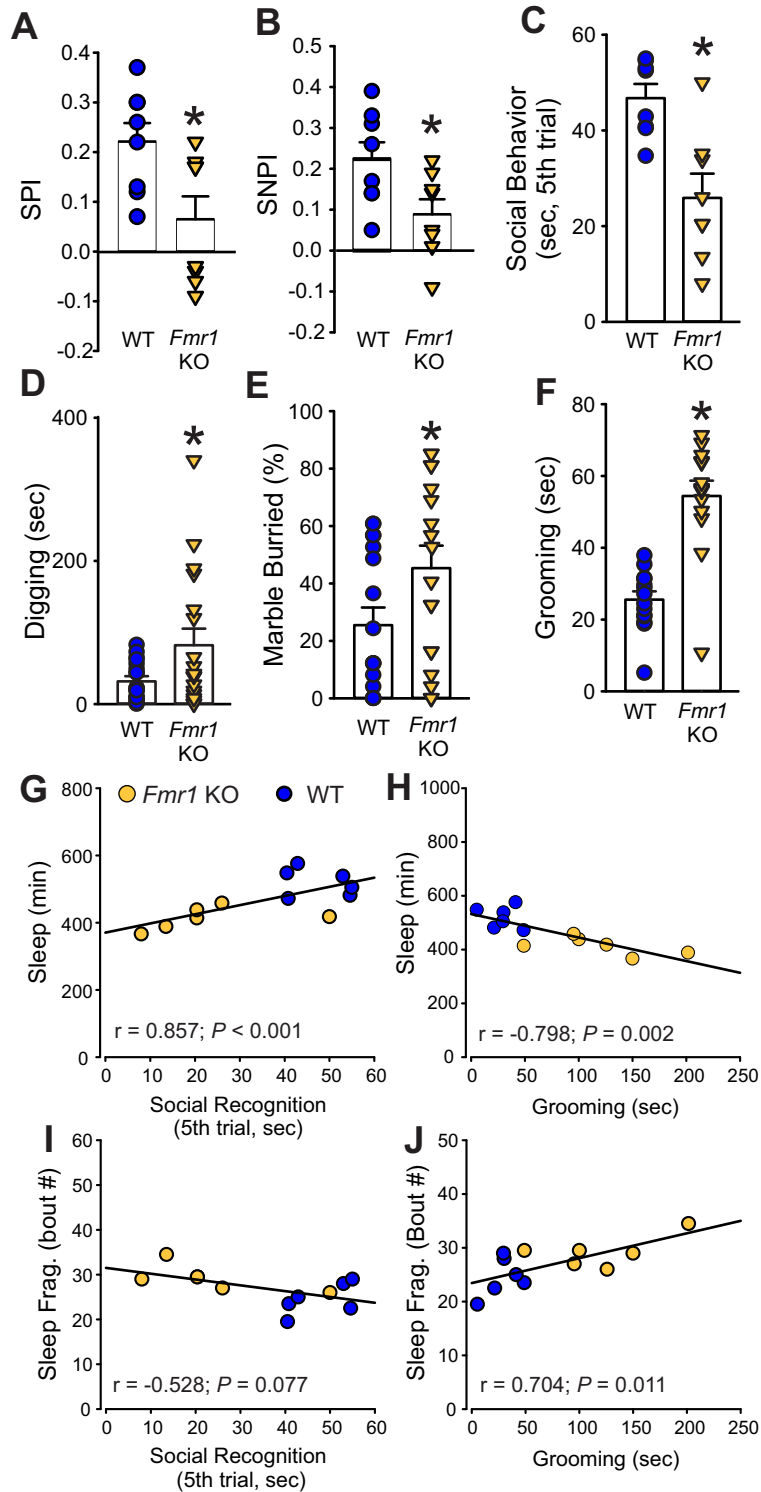


Fig. 7

bioRxiv preprint doi: <https://doi.org/10.1101/2024.09.16.613343>; this version posted September 16, 2024. The copyright holder for this preprint (which was not certified by peer review) is the author/funder, who has granted bioRxiv a license to display the preprint in perpetuity. It is made available under aCC-BY-NC-ND 4.0 International license.

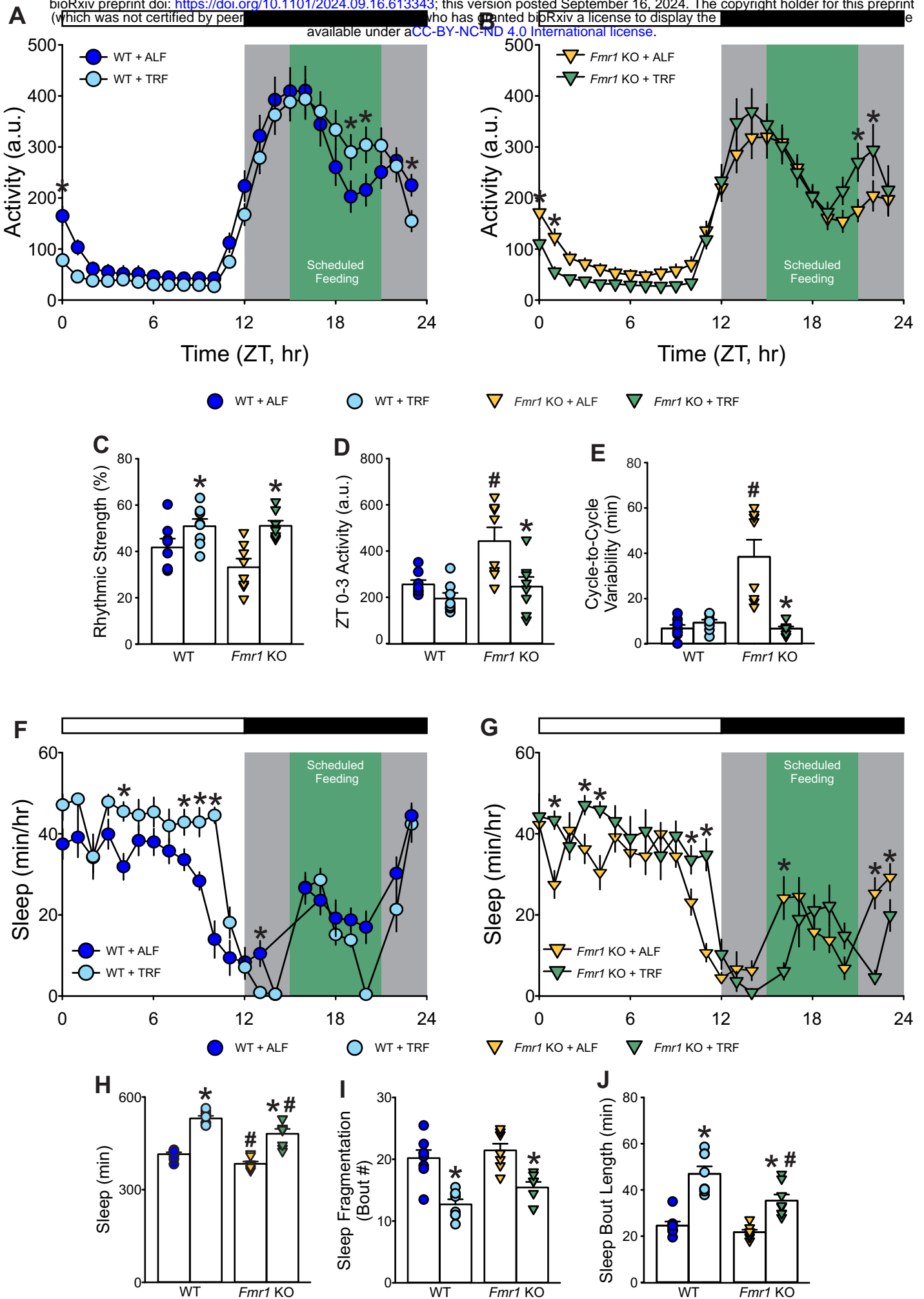


Fig. 8

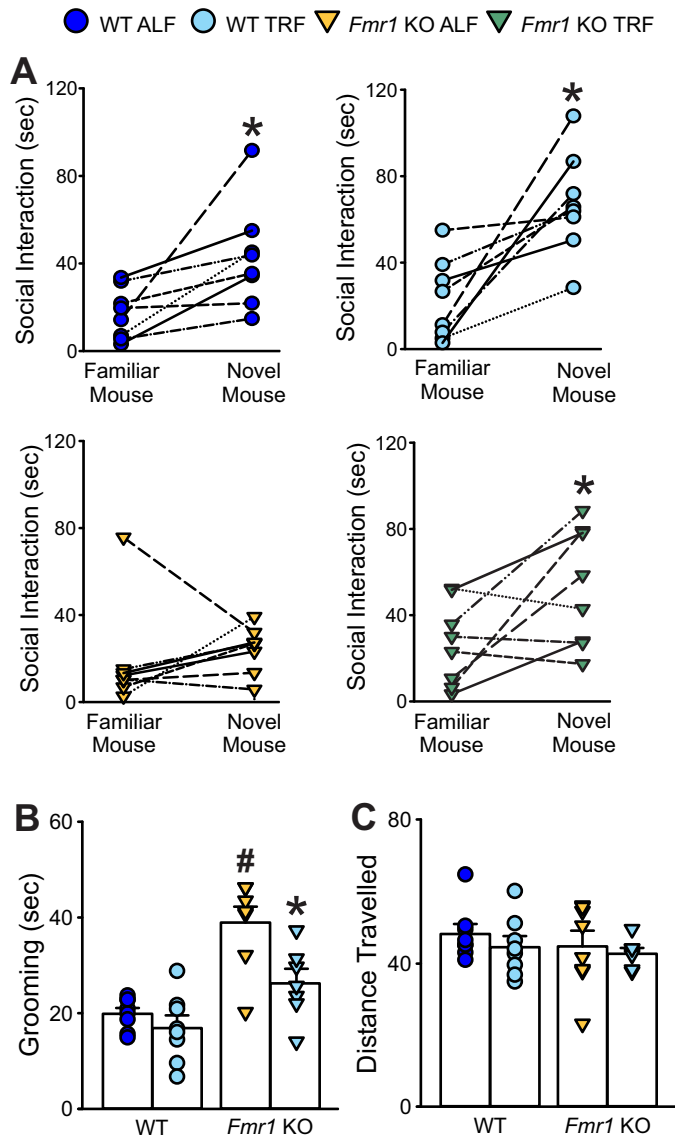


Fig. 9

